Calabrese EJ, Baldwin LA (2002) Applications of hormesis in toxicology, risk assessment and chemotherapeutics. Trends Pharmacol Sci 23(7):331

Chung LY, Cheung TC, Kong SK, Fung KP, Choy YM, Chan ZY, Kwok TT (2001) Induction of apoptosis by green tea catechins in human prostate cancer DU145 cells. Life Sci 68(10):1207

Desbuards N, Hyvelin JM, Machet MC, Eder V, Garrigue MA, Halimi JM, Antier D (2009) Heme oxygenase-1 inducer hemin attenuates the progression of remnant kidney model. Nephron Exp Nephrol 113(1):e35

Furukawa A, Oikawa S, Murata M, Hiraku Y, Kawanishi S (2003) (−)-Epigallocatechin gallate causes oxidative damage to isolated and cellular DNA. Biochem Pharmacol 66(9):1769

Guo Q, Zhao B, Li M, Shen S, Xin W (1996) Studies on protective mechanisms of four components of green tea polyphenols against lipid peroxidation in synaptosomes. Biochim Biophys Acta 1304 (3):210

Hackl C, Mori A, Moser C, Lang SA, Dayoub R, Weiss TS, Schlitt HJ, Geissler EK, Hellerbrand C, Stoeltzing O (2010) Effect of heat-shock protein-90 (HSP90) inhibition on human hepatocytes and on liver regeneration in experimental models. Surgery 147 (5):704

Hosakawa Y, Hosakawa I, Ozaki K, Nakanishi T, Nakane H, Matsuo T (2010) Tea polyphenols inhibit IL-6 production in tumor necrosis factor superfamily 14-stimulated human gingival fibroblasts. Mol Nutr Food Res 54(2):S151

Hu S, Ciancio MJ, Lahav M, Fujiya M, Lichtenstein L, Anant S, Musch MW, Chang EB (2007) Translation inhibition of colonic epithelial heat shock proteins by IFN-gamma and TNF-alpha in intestinal inflammation. Gastroenterology 133(6):1893

Isbrucker RA, Edwards JA, Wolz E, Davidovich A, Bausch J (2006) Safety studies on epigallocatechin gallate (EGCG) preparations. Part 2: dermal, acute and short-term toxicity studies. Food Chem Toxicol 44(5):636

Isemura M, Saeki K, Kimura T, Hayakawa S, Minami T, Sazuka M (2000) Tea catechins and related polyphenols as anti-cancer agents. Biofactors 13(1–4):81

Kankuri E, Hämäläinen M, Hukkanen M, Salmenperä P, Kivilaakso E, Vapaatalo H, Moilanen E (2003) Suppression of pro-inflammatory cytokine release by selective inhibition of inducible nitric oxide synthase in mucosal explants from patients with ulcerative colitis. Scand J Gastroenterol 38(2):186

Keshavarzian A, Sedghi S, Kanofsky J, List T, Robinson C, Ibrahim C, Winship D (1992) Excessive production of reactive oxygen metabolites by inflamed colon: analysis by chemiluminescence probe. Gastroenterology 103(1):177

Kim M, Murakami A, Ohigashi H (2007) Modifying effects of dietary factors on (−)-epigallate-induced pro-matrix metalloproteinase-7 production in HT-29 human colorectal cancer cells. Biosc Biotechnol Biochem 71(10):2442

Kim M, Murakami A, Miyamoto S, Tanaka T, Ohigashi H (2010) The modifying effects of green tea polyphenols on acute colitis and inflammation-association colon carcinogenesis in male ICR mice. Biofactors 36(1):43

Kitajima S, Takuma S, Morimoto M (1999a) Changes in colon mucosal permeability in mouse colitis induced dextran sulfate sodium. Exp Anim 48(3):137

Kitajima S, Takuma S, Morimoto M (1999b) Tissue distribution of dextran sulfate sodium (DSS) in the acute phase of murine DSS-induced colitis. J Vet Med Sci 61(1):67

Köken T, Serteser M, Kahraman A, Akbulut G, Dilek ON (2004) Which is more effective in the prevention of renal ischemia-reperfusion-induced oxidative injury in the early period in mice: interleukin (IL)-10 or anti-IL-12? Clin Biochem 37(1):50

Kweon MH, Adhami VM, Lee JS, Mukhtar H (2006) Constitutive overexpression of Nrf2-dependent heme oxygenase-1 in A549 cells contributes to resistance to apoptosis induced by epigallocatechin 3-gallate. J Biol Chem 281(44):33761

Kwon KH, Murakami A, Hayashi R, Ohigashi H (2005) Interleukin-1 beta targets interleukin-6 in progressing dextran sulfate sodium-induced experimental colitis. Biochem Biophys Res Commun 337(2):647

Lambert JD, Kennett MJ, Sang S, Reuhl KR, Ju J, Yang CS (2010) Yang, C., Hepatotoxicity of high oral dose (−)-epigallocatechin-3-gallate in mice. Food Chem Toxicol 48(1):409

Li C, Li C, Meng X, Winnik B, Lee MJ, Lu H, Sheng S, Buckley B, Yang CS (2001) Analysis of urinary metabolites of tea catechins by liquid chromatography/electrospray ionization mass spectrometry. Chem Res Toxicol 14(6):702

Li Y, Zhang T, Jiang Y, Lee HF, Schwartz SJ, Sun D (2009) (−)-Epigallocatechin-3-gallate inhibits Hsp90 function by impairing Hsp90 association with cochaperones in pancreatic cancer cell line Mia Paca-2. Mol Pharm 6(4):1152

Li GX, Chen YK, Hou Z, Xiao H, Jin H, Lu G, Lee MJ, Liu B, Guan F, Yang Z, Yang CS (2010) Pro-oxidative activities and dose-response relationship of (−)-epigallocatechin-3-gallate in the inhibition of lung cancer growth: a comparative study in vivo and in vitro. Carcinogenesis 31(5):902

Mazzanti G, Menniti-Ippolito F, Moro PA, Cassetti F, Raschetti R, Santuccio C, Mastrangelo S (2009) Hepatotoxicity from green tea: a review of the literature and two unpublished cases. Eur J Clin Pharmacol 65(4):331

Mochizuki M, Hasegawa N (2010) (−)-epigallocatechin 3-gallate reduces experimental colon injury in rats by regulating macrophage and mast cell. Phytother Res 24(S1):S120

Mori T, Ishii T, Akagawa M, Nakamura Y, Nakayama T (2010) Covalent binding of tea catechins to protein thiols: the relationship between stability and electrophilic reactivity. Biosc Biotechnol Biochem 74(12):2451

Musch MW, Ciancio MJ, Sarge K, Chang EB (1996) Induction of heat shock protein 70 protects intestinal epithelial IEC-18 cells from oxidant and thermal injury. Am J Physiol 270(2 Pt 1):C429

Na HK, Kim EH, Jung JH, Lee HH, Hyun JW, Surh YJ (2008) (−)-Epigallocatechin gallate induces Nrf2-mediated antioxidant enzyme expression via activation of PI3K and ERK in human mammary epithelial cells. Arch Biochem Biophys 476(2):171

Nakagawa T, Yokozawa T, Sano M, Takeuchi S, Kim M, Minamoto S (2004) Activity of (−)-epigallocatechin 3-O- gallate against oxidative stress in rats with adenine-induced renal failure. J Agric Food Chem 52(7):2103

Ogborne RM, Rushworth SA, O'Connell MA (2008) Epigallocatechin activates haem oxygenase-1 expression via protein kinase Cδ and Nrf2. Biochem Biophys Res Commun 373(4):584

Ohkawara T, Nishihira J, Takeda H, Miyashita K, Kato K, Kato M, Sugiyama T, Asaka M (2005) Geranylgeranylacetone protects mice from dextran sulfate sodium-induced colitis. Scand J Gastroenterol 40(9):1049

Okayasu I, Hatakeyama S, Yamada M, Ohkusa T, Inagaki Y, Nakaya R (1990) A novel method in the induction of reliable experimental acute and chronic ulcerative colitis in mice. Gastroenterology 98 (3):694

Okushio K, Suzuki M, Matsumoto N, Nanjo F, Hara Y (1999) Methylation of tea catechins by rat liver homogenates. Biosc Biotechnol Biochem 63(2):430

Osburn WO, Wakabayashi N, Misra V, Nilles T, Biswal S, Trush MA, Kensler TW (2006) Nrf2 regulates an adaptive response protecting against oxidative damage following diquat-mediated formation of superoxide anion. Arch Biochem Biophys 454(1):7

Paquay JB, Haenen GR, Stender G, Wiseman SA, Tijburg LB, Bast A (2000) Protection against nitric oxide toxicity by tea. J Agric Food Chem 48(11):5768

Paul G, Battaille F, Obermeier F, Bock J, Klebl F, Strauch U, Lochbaum D, Rümmele P, Farkas S, Schölmerich J, Fleck M, Rogler G, Herfarth H (2005) Analysis of intestinal haem oxygenase-1 (HO-1) in clinical and experimental colitis. Clin Exp Immunol 140(3):547

Rezai-Zadeh K, Aredash GW, Hou H, Fernandez F, Jensen M, Runfeldt M, Shytle RD, Tan J (2008) Green tea epigallocatechin-3-gallate (EGCG) reduces beta-amyloid mediated cognitive impairment and modulates tau pathology in Alzheimer transgenic mice. Brain Res 1214(12):177

Sahin K, Tuzuc M, Gencoglu H, Dogukan A, Timurkan M, Sahin N, Aslan A, Kucuk O (2010) Epigallocatechin-3-gallate activates Nrf2/HO-1 signaling pathway in cisplatin-induced nephrotoxicity in rats. Life Sci 87(7–8):240

Sang S, Lambert JD, Hong J, Tian S, Lee MJ, Stark RE, Ho CT, Yang CS (2005) Synthesis and structure identification of thiol conjugates of (−)-epigallocatechin gallate and their urinary levels in mice. Chem Res Toxicol 18(11):1762

Shi Q, Domg Z, Wei H (2007) The involvement of heat shock proteins in murine liver regeneration. Cell Mol Immunol 4(1):53

Suganuma M, Okabe S, Oniyama M, Tada Y, Ito H, Fujiki H (1998) Wide distribution of [^{3}H] (−)-epigallocatechin gallate, a cancer preventive tea polyphenol, in mouse tissue. Carcinogenesis 19 (10):1771

Tanaka K, Namba T, Arai Y, Fujimoto M, Adachi H, Sobue G, Takeuchi K, Nakai A, Mizushima T (2007) Genetic evidence for a protective role for heat shock factor 1 and heat shock protein 70 against colitis. J Biol Chem 282(32):23240

Tran PL, Kim SA, Choi HS, Yoon JH, Ahn SG (2010) Epigallocatechin-3-gallate suppresses the expression of HSP70 and HSP90 and exhibits anti-tumor activity in vitro and in vivo. BMC Cancer 10:276. doi:10.1186/1471-2407-10-276

Wang WP, Guo X, Koo MW, Wong BC, Lam SK, Ye YN, Cho CH (2001) Protective role of heme oxygenase-1 on trinitrobenzene sulfonic acid-induced colitis in rats. Am J Physiol Gastrointest Liver Physiol 281(2):G586

Wang JS, Luo H, Wang P, Tang L, Yu J, Huang T, Cox S, Gao W (2008) Validation of green tea polyphenol biomarkers in a phase II human intervention trial. Food Chem Toxicol 46(1):232

Wischmeyer PE, Musch MW, Madonna MB, Thisted R, Chang EB (1997) Glutamine protects intestinal epithelial cells: role of inducible HSP70. Am J Physiol Gastrointest Liver Physiol 272(4 Pt 1):G879

Xue H, Sufit AJ, Wischmeyer PE (2011) Glutamine therapy improves outcome of in vitro and in vivo experiment colitis models. JPEN J Parenter Enteral Nutr 35(2):188

Yamabe N, Yokozawa T, Oya T, Kim M (2006) Therapeutic potential of (−)-epigallocatechin 3-O- gallate on renal damage in diabetic nephropathy model rats. J Pharmacol Exp Ther 319(1):228

As mentioned above, EGCG undergoes autoxidation to generate ROS. Oxidized EGCG in the B-ring is non-enzymatically converted to an EGCG *o*-quinone, which rapidly reacts with glutathione or protein thiols via covalent bindings (Mori et al. 2010). Thus, it is conceivable that administration of high-dose GTPs leads to accumulation of EGCG *o*-quinone, which escapes from inactivation processes by metabolism. These bioactive electrophiles may be responsible for inducing toxicity in the liver and kidneys. In fact, formation of EGCG-thiol conjugates was detected only at high doses (400 mg/kg) following intraperitoneal injection in mice (Sang et al. 2005). Meanwhile, high-dose EGCG reduced the expressions of antioxidant enzymes, including HO-1, SOD, and catalase (Kweon et al. 2006; Kim et al. 2010). Along a similar line, our present results revealed that 1% GTPs dramatically decreased the mRNA expressions of HO-1 and NQO1 in the kidneys and livers of non-treated mice (Fig. 5b, c). It is of great importance to point out that HO-1 was reported to attenuate the progression of chronic kidney disease (Desbuards et al. 2009). Therefore, we assume that high-dose GTPs act not only in a pro-oxidant manner, but also down-regulate antioxidant enzymes, leading to hepatic and renal dysfunctions.

It is interesting that down-regulation of HSP70 has been found to be associated with IBD development (Bhattacharrya et al. 2009; Köken et al. 2004; Hu et al. 2007). Although we also reported that a 1% GTPs diet aggravated colitis in DSS-exposed mice (Kim et al. 2010), it was not clear whether 1% GTPs affected the expression HSP70 in that model. In our present study, renal and hepatic HSP70 expressions were dramatically suppressed by DSS exposure, while the 1% GTPs diet did not affect those in DSS-induced colitis mice. On the other hand, it should be noted that 1% GTPs treatment decreased hepatic HSP70 by 21% as compared with the non-treated mice (Fig. 6b). Anwar et al. showed that HSP70 interacts with an unfolded form of NQO1 and thereby inhibited its degradation (Anwar et al. 2002), implying a supporting role of HSP70 in NQO1 stabilization. In support of that notion, the expression patterns of HSP70 and NQO1 in the present four groups were positively correlated, except for data from the kidneys in group 2 (Figs. 5c and 6b). Renal and hepatic HSP27 levels were also remarkably down-regulated by the combination of GTPs and DSS (Fig. 6c). Thus, the 1% GTPs diet might have induced hepatic and renal toxicity, at least in part, by attenuating the expressions of both HSP70 and HSP27. More strikingly, HSP90 in kidneys and livers of the non-treated mice was identified as a chaperone protein that is hyper-sensitive to GTPs (Fig. 6d). These results are consistent with those of Tran et al., who previously found that HSP90 was repressed by EGCG in MCF-7 human breast cancer cells (Li et al. 2009; Tran et al. 2010). Because HSP90 is the most abundant molecular chaperone and plays pivotal roles in maintaining organ homeostasis (Shi et al. 2007; Hackl et al. 2010), its down-regulation by GTPs might be associated with organ dysfunction and toxicity. In addition, it is significant to note that increased HSP70 expression by both glutamine and geranylgeranylacetone contributed to the protection against inflammation including IBD (Ohkawara et al. 2005; Xue et al. 2011).

The present 1% GTPs diet, which contained 35% EGCG, decreased survival rates (Fig. 2a) and down-regulated antioxidant and xenobiotic-metabolizing enzymes in mice with DSS-induced colitis (Fig. 5a). In contrast, we previously reported that a low-dose GTPs (0.1~0.25%) diet had a tendency to improve both ulcers and inflammation in a colitis model (Kim et al. 2010). Therefore, low or moderate doses of GTPs may exhibit beneficial effects toward DSS-induced hepatotoxicity and nephrotoxicity. This hypothesis may be supported by Calabrese and Baldwin who described the U-shaped toxicity of environmental chemicals (Calabrese and Baldwin 2002).

Taken together, our findings indicate that a high-dose GTPs diet exacerbates kidney and liver functions, presumably through down-regulation of antioxidant enzymes and HSPs, in both normal mice and those with DSS-induced colitis. The effects of low and medium dose of GTPs diets on these functions are now being investigated in our laboratory.

Acknowledgements This work was supported by the Programme for Promotion of Basic and Applied Researches for Innovations in Bio-oriented Industry and by Research and Development Projects for Application in Promoting New Policy of Agriculture Forestry and Fisheries, Ministry of Agriculture, Forestry and Fisheries, Japan (Grant No. 23005).

References

Abboud PA, Hake PW, Burroughs TJ, Odoms K, O'Connor M, Mangeshkar P, Wong HR, Zingarelli B (2008) Therapeutic effect of epigallocatechin-3-gallate in a mouse model of colitis. Eur J Clin Pharmacol 579(1–3):411

Anwar A, Siegel D, Kepa JK, Ross D (2002) Interaction of the molecular chaperone Hsp70 with human NAD(P)H:quinone oxidoreductase 1. J Biol Chem 277(16):14060

Araki Y, Andoh A, Fujiyama Y (2003) The free radical scavenger edaravone suppresses experimental dextran sulfate sodium-induced colitis in rats. Int J Mol Med 12(1):125

Araki Y, Mukaisyo K, Sugihara H, Fujiyama Y, Httori T (2010) Increased apoptosis and decreased proliferation of colonic epithelium in dextran sulfate sodium-induced colitis in mice. Oncol Rep 24(4):869

Bhattacharrya S, Dudeja PK, Tobacman JK (2009) ROS, HSP27, and IKKbeta mediate dextran sodium sulfate (DSS) activation of Ikappaba, NFKappaB, and IL-8. Inflamm Bowel Dis 15(5):673

Cai EP, Lin JK (2009) Epigallocatechin gallate (EGCG) and rutin suppress the glucotoxicity through activating IRS2 and AMPK signaling in rat pancreatic beta cells. J Agric Food Chem 57 (20):9817

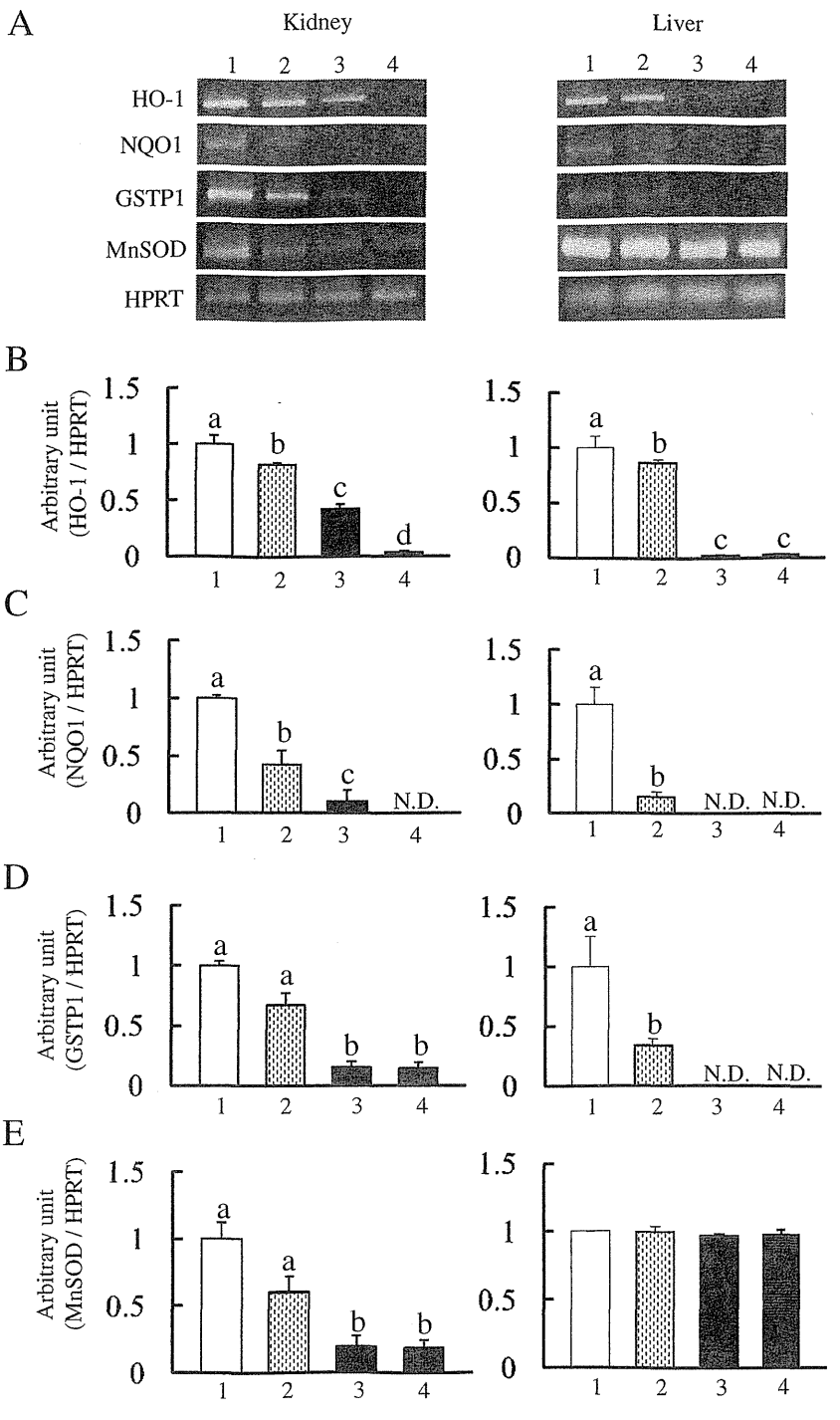

Fig. 5 Effects of DSS and/or 1% GTPs supplementation on antioxidant enzyme mRNA levels in mouse kidneys and livers. *HO-1*, *NQO1*, *GSTP1*, and *MnSOD* mRNA expressions were determined by RT-PCR (**a**), with representative findings presented. Densitometric quantification of HO-1 (**b**), NQO1 (**c**), GSTP1 (**d**), and MnSOD (**e**) was performed used NIH Image. *HPRT* was used as an internal control. *N.D.* indicates not detected. Data are shown as the mean±SD of ten samples. *Bars with different letters* show significant differences ($P<0.05$)

the other hand, several recent studies have also noted that excess intake of green tea supplements induced hepatotoxicity in both rodents and humans (Lambert et al. 2010; Mazzanti et al. 2009; Isbrucker et al. 2006). In addition, the present study showed for the first time that high-dose GTPs caused nephrotoxicity in mice as observed by increased serum creatinine level (Fig. 4d). In support of those findings, it is well known that GTPs and EGCG function as pro-oxidants in vivo and in vitro, and exhibit genotoxicity and tumor promotional potentials (Li et al. 2010; Kim et al. 2010; Furukawa et al. 2003; Guo et al. 1996). However, the molecular mechanisms underlying their potential toxicity have not been fully elucidated.

A recent study by Lambert et al. reported that intragastric administration of high-dose EGCG (1,500 mg/kg) caused hepatotoxicity in mice (Lambert et al. 2010), while we

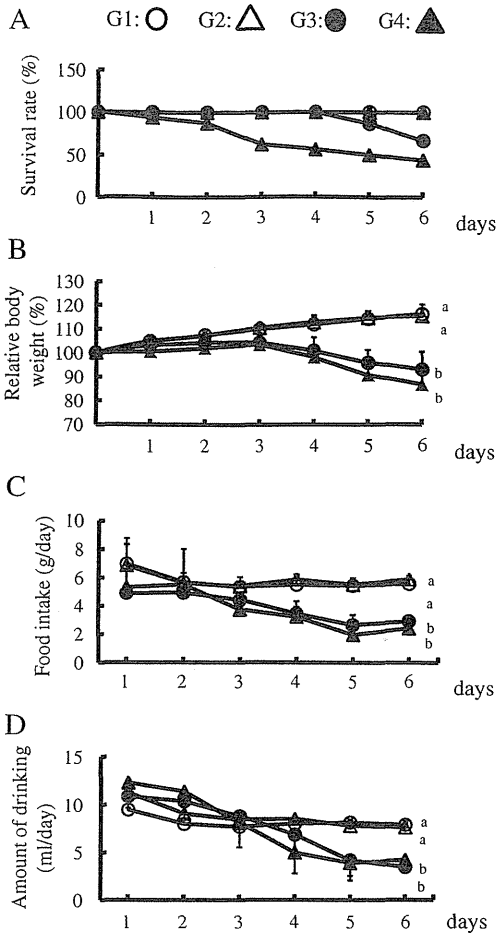

Fig. 2 Effects of DSS and/or 1% GTPs supplementation on survival (**a**), relative body weight (**b**), food intake (**c**), and water intake (**d**). Group 1 (n=15) (*white circle*), group 2 (n=15) (*white triangle*), group 3 (n=15) (*black circle*), group 4 (n=17) (*black triangle*). Data are shown as the mean±SD. Values with different letters are significantly different, $p<0.05$

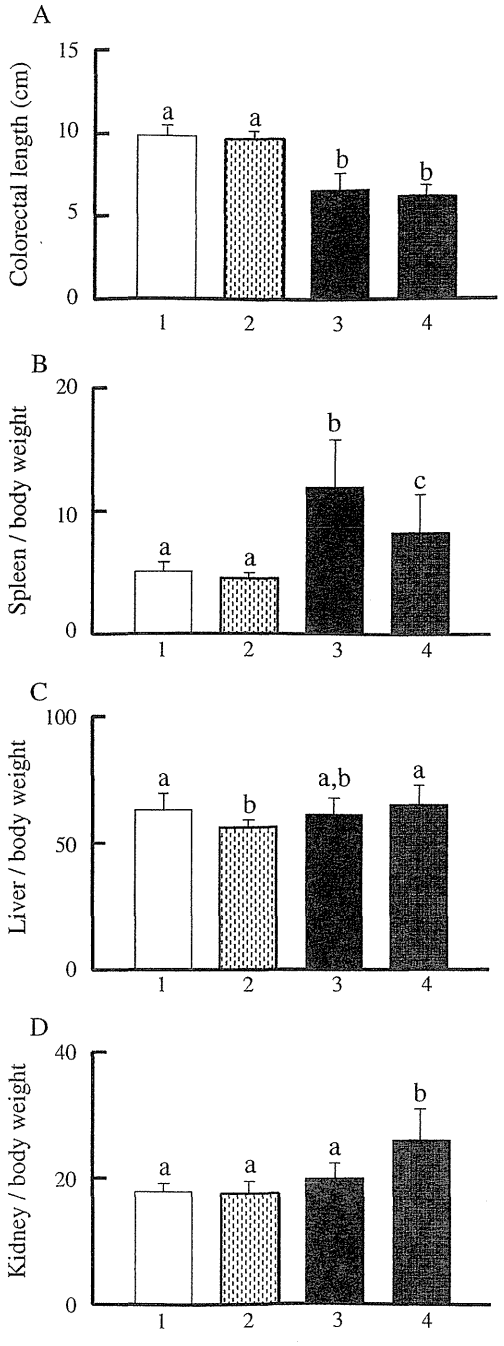

Fig. 3 Effects of DSS and/or 1% GTPs supplementation on organs. Colon length (**a**), spleen weight (**b**), liver weight (**c**), and kidney weight (**d**) were determined. Group 1 (n=15), group 2 (n=15), group 3 (n=15), group 4 (n=17). Data are shown as the mean±SD. *Bars with different letters* show significant differences ($P<0.05$)

Hepatic and renal function parameters and lipid peroxidation level

Serum AST and ALT levels, which reflect hepatic functions, were also measured. DSS (group 3) markedly increased both parameters as compared to no treatment (group 1), while 1% GTP (group 2) did not have a significant effect (Fig. 4a, b). Elevation of TBARS is a reliable indicator of lipid peroxidation, which might be closely related to tissue damage (Lambert et al. 2010). As shown in Fig. 4c, the hepatic TBARS level in group 4 was significantly greater (1.9-fold) than that in group 3. Similarly, we found a significant increase in group 2 as compared to group 1. Next, we measured serum creatinine levels as a biomarker of renal function (Nakagawa et al. 2004). Although DSS exposure did not have an effect on serum creatinine (group 1 vs. group 3), the serum creatinine level in group 4 was dramatically increased (2.9-fold) as compared to group 3 (Fig. 4d). Furthermore, TBARS levels in the kidneys of mice fed with the GTPs diet (groups 2 and 4) were markedly elevated than in those of their respective controls (groups 1 and 3; Fig. 4e).

(Tanaka et al. 2007). In addition, several studies have demonstrated that inhibition of an antioxidant enzyme, heme oxygenase-1 (HO-1), leads to aggravation of DSS-induced colitis (Paul et al. 2005; Wang et al. 2001).

Heat shock proteins (HSPs) are a class of stress-inducible proteins that play roles as molecular chaperones and protect cells against proteotoxic damage from a variety of physiological and environmental stimuli (Musch et al. 1996; Wischmeyer et al. 1997). Interestingly, the expressions of HSP70 and HSP27 were found to be down-regulated in actively inflamed mucosa from individuals with IBD (Bhattacharrya et al. 2009; Köken et al. 2004). It is worth noting that the production of pro-inflammatory cytokines, such as tumor necrosis factor (TNF)-α and interleukin, were also found to be increased in IBD, while it down-regulated HSP70 by targeting its translation stage (Hu et al. 2007). The above background suggests that inflammatory signaling molecules aggravate colitis by down-regulating HSPs, thereby disrupting intestinal homeostasis.

Green tea is a popular and widely consumed beverage. It contains characteristic polyphenolic constituents, generally known as green tea polyphenols (GTPs), which include (−)-epigallocatechin-3-gallate (EGCG), (−)-epicatechin gallate, (−)-epigallocatechin, and (−)-epicatechin. (Isemura et al. 2000). EGCG, the most abundant polyphenol, has versatile preventive effects toward several chronic diseases including cancer, inflammation, heart disease, diabetes, and neurodegenerative diseases (Chung et al. 2001; Li et al. 2010; Hosakawa et al. 2010; Suganuma et al. 1998; Paquay et al. 2000; Cai and Lin 2009; Rezai-Zadeh et al. 2008). In addition, GTPs are strong antioxidants against ROS as well as inducers of several antioxidant proteins [HO-1, NAD(P)H:quinone oxidoreductase 1 (NQO1), glutathione *S*-transferase pi (GSTP1), manganese superoxide dismutase] (Sahin et al. 2010; Ogborne et al. 2008; Na et al. 2008).

Recently, high-dose EGCG was reported to induce hepatotoxicity, as demonstrated by increased formation of malonyldialdehyde (MDA) and 4-hydroxynonenal (4-HNE) (Lambert et al. 2010). Along a similar line, we found that EGCG enhanced the expression of pro-matrix metalloproteinase-7 by inducing oxidative stress in HT-29 human colorectal cancer cells (Kim et al. 2007). Furthermore, a 1% GTP diet enhanced pro-inflammatory cytokines, aggravated colitis, and tended to promote colon carcinogenesis in DSS-exposed colons, while it decreased the activities of superoxide dismutase (SOD) and catalase in non-treated mice (Kim et al. 2010). In addition, several human cases of hepatotoxicity following consumption of dietary supplementation containing green tea extracts have been reported (Mazzanti et al. 2009).

In the present study, oral feeding of 1% GTPs caused kidney and liver dysfunctions, as revealed by increases in serum aspartate 2-oxoglutarate aminotransferase (AST), alanine aminotransferase (ALT), and creatinine, as well as thiobarbituric acid-reactive substances (TBARS) levels in kidneys and livers, together with down-regulation of antioxidant enzymes and HSPs, in both normal and DSS-treated ICR mice.

Materials and methods

Chemicals

A GTP mixture containing 70% total catechins, 35% EGCG, and 3% caffeine was obtained from LKT laboratories, (West St. Paul, MN). DSS with a molecular weight of 36–50 kDa was purchased from MP Biomedicals, (LLC Aurora, OH). All other chemicals and kits were obtained from Wako Pure Chemical Industries (Osaka, Japan), unless specified otherwise.

Animals

Male-specific pathogen-free ICR mice (17–19 g, 4 weeks old) were purchased from Japan SLC (Shizuoka, Japan) and housed five per cage. All mice were fed rodent MF pellets (Oriental Yeast, Kyoto, Japan) and given fresh tap water ad libitum, while being kept at 22–26°C with a relative humidity of 55–65% under a 12-h (0600–1800 hours) light/dark cycle for 6 days prior to the experiment. The mice were treated in accordance with the "Guidelines for the Treatment of Experimental Animals" of Kyoto University and the experimental protocol was approved by the Experimentation Committee of the same institution (approval number 21-42).

Experimental design

The experimental design is illustrated in Fig. 1. Mice were randomly divided into four groups: non-treated (group 1), GTPs-treated (group 2), DSS-treated (group 3), and GTPs + DSS-treated (group 4). The GTP-fed groups were given a diet containing 1% GTPs. DSS-treated groups were given 5% DSS (*w/v*) in water ad libitum, which induced experimental colitis. Body weights and food intake of each group were recorded each day until the end of experiment. All mice were euthanized by deep anesthesia with diethyl ether for determining the effects of dietary GTPs on DSS-induced colitis.

RNA extraction and reverse transcription polymer chain reaction analysis

Total RNA was prepared using Trizol (Invitrogen, Tokyo, Japan), as described in the manufacturer's instructions. For reverse transcription (RT-PCR) analysis, 1 μg of RNA was reverse transcribed using an RNA PCR kit (TaKaRa, Shiga, Japan) with oligo dT-adaptor primer, as recommended by the supplier. PCR was done using a thermal cycler (PTC-0100;

Published OnlineFirst May 16, 2011; DOI:10.1158/1940-6207.CAPR-11-0188

Research Article

Cancer Prevention Research

Selective PGE_2 Suppression Inhibits Colon Carcinogenesis and Modifies Local Mucosal Immunity

Masako Nakanishi[1], Antoine Menoret[2], Takuji Tanaka[3], Shingo Miyamoto[1], David C. Montrose[1], Anthony T. Vella[2], and Daniel W. Rosenberg[1]

Abstract

Prostaglandin E_2 (PGE_2) is a bioactive lipid that mediates a wide range of physiologic effects and plays a central role in inflammation and cancer. PGE_2 is generated from arachidonic acid by the sequential actions of the COX and terminal synthases (PGES). Increased levels of COX-2, with a concomitant elevation of PGE_2, are often found in colorectal cancers (CRC), providing the rationale for the use of COX-2 inhibitors for chemoprevention. Despite their proven efficacy in cancer prevention, however, COX-2 inhibitors exhibit dose-dependent toxicities that are mediated in part by their nonspecific reduction of essential prostanoids, thus limiting their chemopreventive benefit. To achieve enhanced specificity, recent efforts have been directed toward targeting the inducible terminal synthase in the production of PGE_2, microsomal PGES (mPGES-1). In the present study, we show that genetic deletion of *mPGES-1* affords significant protection against carcinogen-induced colon cancer. *mPGES-1* gene deletion results in an about 80% decrease in tumor multiplicity and up to a 90% reduction in tumor load in the distal colon of azoxymethane (AOM)-treated mice. Associated with the striking cancer suppression, we have identified a critical role for PGE_2 in the control of immunoregulatory cell expansion (FoxP3-positive regulatory T cells) within the colon-draining mesenteric lymph nodes, providing a potential mechanism by which suppression of PGE_2 may protect against CRC. These results provide new insights into how PGE_2 controls antitumor immunity. *Cancer Prev Res; 4(8); 1198–208. ©2011 AACR.*

Introduction

Selective inhibition of prostaglandin E_2 (PGE_2) synthesis via pharmacologic targeting of mPGES-1 may provide chemopreventive efficacy while limiting the toxicity that is often associated with long-term use of COX-2 inhibitors (1). mPGES-1 is an inducible terminal synthase with only moderate expression under normal physiologic conditions (2). However, coordinated induction of mPGES-1 and COX-2 is often observed within a variety of cancer types (3). Our laboratory recently reported that genetic deletion of *mPGES-1* in *Apc* mutant mice significantly suppressed intestinal tumorigenesis, a protective effect that occurred in the absence of significant metabolic shunting of the COX-2 product, PGH_2, to other prostaglandins (4).

Authors' Affiliations: [1]Center for Molecular Medicine, [2]Department of Immunology, University of Connecticut Health Center, Farmington, Connecticut; and [3]Tohkai Cytopathology Institute: Cancer Research and Prevention, Gifu, Japan

Note: Supplementary data for this article are available at Cancer Prevention Research Online (http://cancerprevres.aacrjournals.org/).

Corresponding Author: Daniel W. Rosenberg, Center for Molecular Medicine, University of Connecticut Health Center, 263 Farmington Avenue, Farmington, CT 06030. Phone: 1-860-679-8704; Fax: 1-860-679-7639; E-mail: Rosenberg@nso2.uchc.edu

doi: 10.1158/1940-6207.CAPR-11-0188

Despite the profound suppression in tumor formation that was observed in this earlier study, the effect of *mPGES-1* deletion in the colon was less apparent due to the propensity of *Apc* mutant mice to develop tumors in the small intestine (5). To address the issue of tissue specificity, we introduced the *mPGES-1* gene deletion onto strain A mice, a line that is highly sensitive to chemical-induced colon cancer (6–8). In the following study, we examined the impact of *mPGES-1* genetic status on colon carcinogenesis induced by azoxymethane (AOM), an organospecific carcinogen that causes multiple adenomas in the distal colon (8). Genetic deletion of *mPGES-1* affords significant protection against AOM-induced colon cancer. Associated with the striking cancer protection, we identified a critical role for PGE_2 in the control of immunoregulatory cell expansion [FoxP3-positive regulatory T cells (Treg)] within the colon-draining mesenteric lymph nodes (MLN), providing a potential mechanism by which inhibition of mPGES-1 and inducible PGE_2 synthesis may protect against colorectal cancers (CRC).

Materials and Methods

Generation of *mPGES-1* deletion on A/J background

Male A/J mice were purchased from The Jackson Laboratory and crossed with female *mPGES-1* knockout (KO) mice (C57BL/6; ref. 9). *mPGES-1* heterozygous mice were backcrossed onto A/J mice for 9 additional generations

Published OnlineFirst May 16, 2011; DOI:10.1158/1940-6207.CAPR-11-0188

(N10). N10 heterozygous mice were intercrossed to generate A/J:*mPGES-1* KO mice. Genotyping was carried out by tail biopsy. Mice were maintained in a temperature-controlled, light-cycled room and allowed free access to drinking water and standard diet (LM-485; Harlan Teklad).

AOM treatment

Six-week-old wild-type (WT) and KO mice were injected intraperitoneally with AOM (10 mg/kg of body weight; Sigma-Aldrich) or vehicle control (0.9% NaCl) once a week for a total of 6 weeks. Twenty weeks after the last injection, mice were sacrificed and blood, spleen, MLNs, and colon were harvested for further analysis. Colons were flushed immediately with ice-cold PBS and excised longitudinally. Specimens were fixed flat in 10% neutral buffered formalin for 4 hours and stored in 70% ethanol. Animal experiments were conducted after approval by the Animal Care Committee (ACC/IACUS) at the University of Connecticut Health Center.

Quantification of lesions

Whole-mount colons were stained with 0.2% methylene blue and the number and size of aberrant crypt foci (ACF) and tumors were scored under a dissecting microscope. Colon tumor load per mouse was determined using tumor diameter to calculate the spherical tumor volume ($V = 4/3\ \pi\ r^3$). The amount of ulcerated tissue was determined as the percentage across the entire length of colon ($n = 10$ per group).

Immunohistochemistry

Colons were paraffin embedded and sectioned at 5-μm thickness. Sections were treated with 1% to 3% hydrogen peroxide, blocked, and incubated with anti-APC (1:800; Millipore), anti-PCNA (1:150; Novocastra Laboratories Ltd.), anti-PECAM1 (1:500; Santa Cruz Biotechnologies, Inc.), anti-β-catenin (1:2,000; Sigma-Aldrich), anti-cleaved caspase-3 (1:200; Cell Signaling Technology Inc.), anti-cyclinD1 (1:20; Novus Biologicals), anti-mPGES-1 (1:5,000; Abnova), and anti-Ki-67 (1:50; Dako North America, Inc.). Sections were incubated with biotinylated secondary antibody, followed by ABC reagent (Vector Laboratories Inc.). Signal was detected using 3,3′-diaminobenzidine (DAB) solution (Vector Laboratories). Tissues were counterstained with hematoxylin.

Immunofluorescence microscopy

Following antigen retrieval, sections were blocked and incubated with anti-mPGES-1 (1:5,000; Abnova) and then incubated with secondary antibody conjugated with Cy5 (1:500; Millipore). Nuclei were stained with Sytox Orange (1:10,000; Invitrogen). Staining was visualized by confocal microscopy using a Zeiss LSM 510/Confocor II and images were analyzed by LSM image browser software.

Flow cytometry

RBC-depleted spleens and MLN cells were resuspended with staining buffer (balanced salt solution, 3% FBS and 0.1% sodium azide), followed by blocking solution containing normal mouse serum, anti-Fc receptor supernatant from the 2.4 G2 hybridoma (10), and human γ-globulin. Cells were incubated with labeled primary antibodies (CD4, CD8, CD11b, Gr-1 from eBioscience; Ki-67 from BD Biosciences) and analyzed by flow cytometry as described before (11). Intracellular staining of FoxP3 was conducted according to manufacturer's protocol (eBioscience).

In vitro lymphocytes stimulation

Spleens and MLNs were harvested from 20- to 25-week-old untreated female A/J mice, and 1×10^6 cells were stimulated with phorbol-12-myristate-13-acetate (PMA; 50 ng/mL; Sigma) and ionomycin (1 μg/mL; Sigma) for 4 hours in the presence of Brefeldin A (10 μg/mL; Sigma). Intracellular staining was conducted for interleukin (IL) 10, IFN-γ, and Foxp3 (eBioscience,) as described earlier ($n = 6$ per group).

Histologic evaluation

Colon histology was evaluated on Swiss-rolled hematoxylin and eosin (H&E) sections by a board-certified pathologist (T.T.). Colonic crypt dysplasia was diagnosed according to established criteria (12), and colon tumors were further diagnosed using histopathologic descriptions (13).

PGE_2 and serum cytokine analyses

Serum was prepared from blood and samples were purified using a PGE_2 affinity column (Cayman Chemical). PGE_2 concentrations were determined by ELISA (Cayman Chemical; $n = 13$ per group). Serum cytokine levels were determined using a Bio-Plex Pro assay (Bio-Rad Laboratories, Inc.; $n = 5$ per group).

Measurement of the proliferative zone

Quantification of the proliferative zone was assessed on proliferating cell nuclear antigen (PCNA)-stained tissues, randomly selecting 25 crypts per mouse for analysis ($n = 5$ per group). The ratio of positive cells to total cells within the crypt was calculated for each colon, and an average of the ratios were compared between WT and *mPGES-1* KO mice.

Statistical analyses

Statistical analyses of tumor size and multiplicity, as well as a comparison of PGE_2 levels and the frequency of immune cells using fluorescence-activated cell-sorting (FACS) analysis, were conducted by Student's *t* test. A value of $P < 0.05$ was considered statistically significant.

Results

mPGES-1 deletion suppresses colon carcinogenesis

mPGES-1 KO mice and WT littermates were injected with AOM and colons were harvested for analysis 20 weeks after the last injection. In response to AOM treatment, WT mice

Published OnlineFirst May 16, 2011; DOI:10.1158/1940-6207.CAPR-11-0188

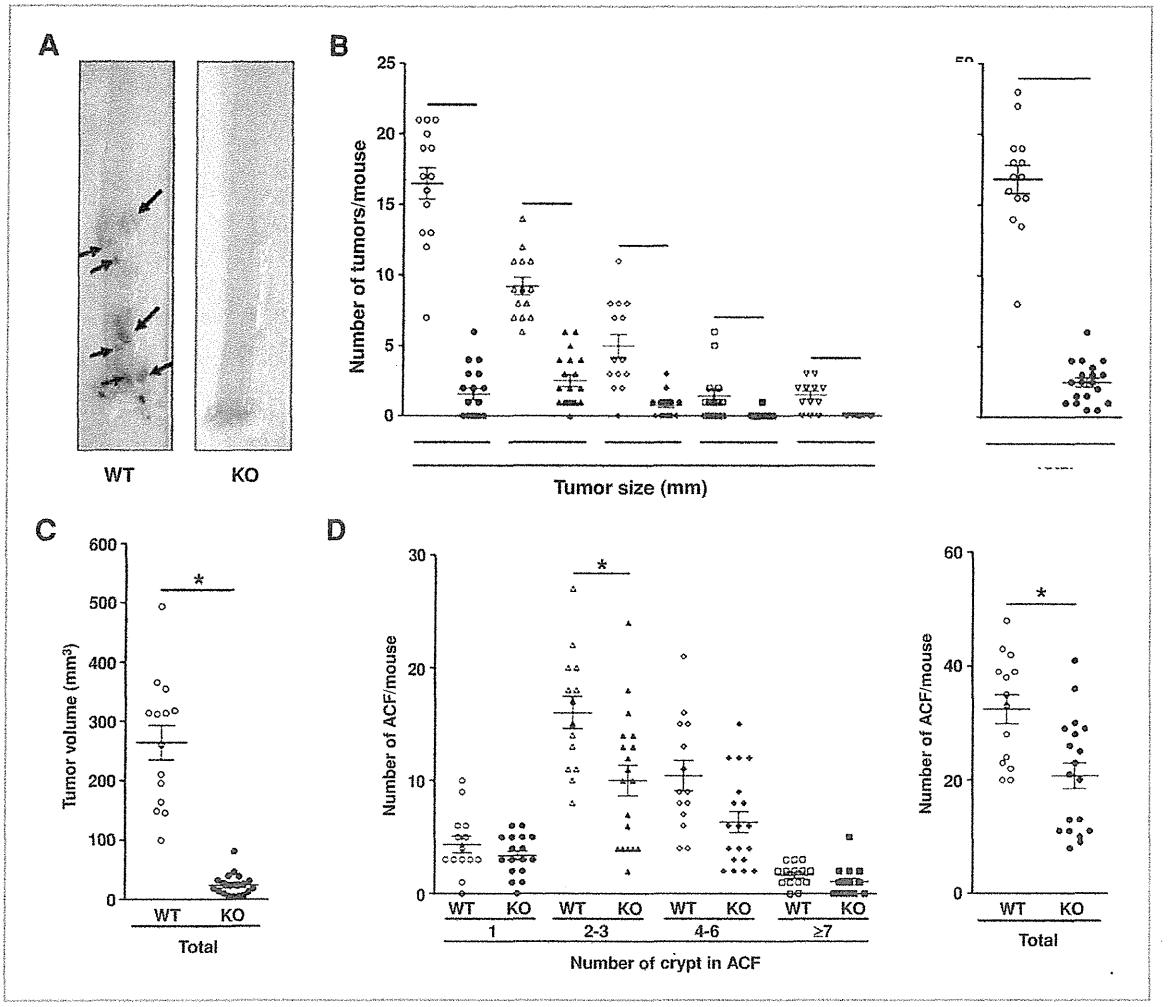

Figure 1. Genetic deletion of *mPGES-1* suppresses AOM-induced colon cancer. A, representative whole-mount colons showing numerous large, well-vascularized tumors in the WT mice (arrows). B, size distribution and total number of tumors per colon rounded to the nearest whole number, as well as total tumor volume (mm^3). C, size distribution and total number of ACF. Each data point represents an individual mouse. Bars indicate means ± SEM. *, $P < 0.05$ compared with WT mice.

developed multiple, large, and highly vascularized tumors, primarily confined to the distal colon (Fig. 1A, arrows). In *mPGES-1* KO mice, however, only several colons had macroscopically visible tumors (Fig. 1A). Tumor enumeration revealed a remarkable suppression (up to 85%) in *mPGES-1* KO mice (33.6 ± 2.0 vs. 5.0 ± 0.7 in WT and KO, respectively; $P < 0.0001$; Fig. 1B), whereas tumor load was reduced by up to 90% (264.0 ± 29.0 vs. 24.3 ± 4.3 in WT and KO, respectively; $P < 0.0001$; Fig. 1C). Despite the virtually complete protection against tumor formation, the total number of ACF, a preneoplastic lesion common to the distal colon, was reduced by less than 40% (32.4 ± 2.5 vs. 20.7 ± 2.3 in WT and KO, respectively; $P < 0.002$; Fig. 1D). The most effective protection occurred in ACF of intermediate size, including those with 2 to 3 (16.0 ± 1.4 vs. 10.0 ± 1.4 in WT and KO, respectively; $P < 0.005$) and 4 to 6 crypts per focus (10.4 ± 1.3 vs. 6.3 ± 0.9 in WT and KO, respectively; $P < 0.01$).

In WT mice, analysis of tumor histology identified primarily 2 forms of large adenomas, characterized by either a pedunculated or flat morphology (Fig. 2, WT). The tubular adenomas often exhibited an elongated structure with a stalk (Fig. 2, arrow). In the *mPGES-1* KO mice, however, only 1 of 19 mice developed a large adenoma (>3 mm), which had either a flat or a slightly raised morphology (Fig. 2, KO). Microadenomas were found in the colons from either genotype, although carcinomas *in situ* were limited to the WT mice (Fig. 2, WT). The

Published OnlineFirst May 16, 2011; DOI:10.1158/1940-6207.CAPR-11-0188

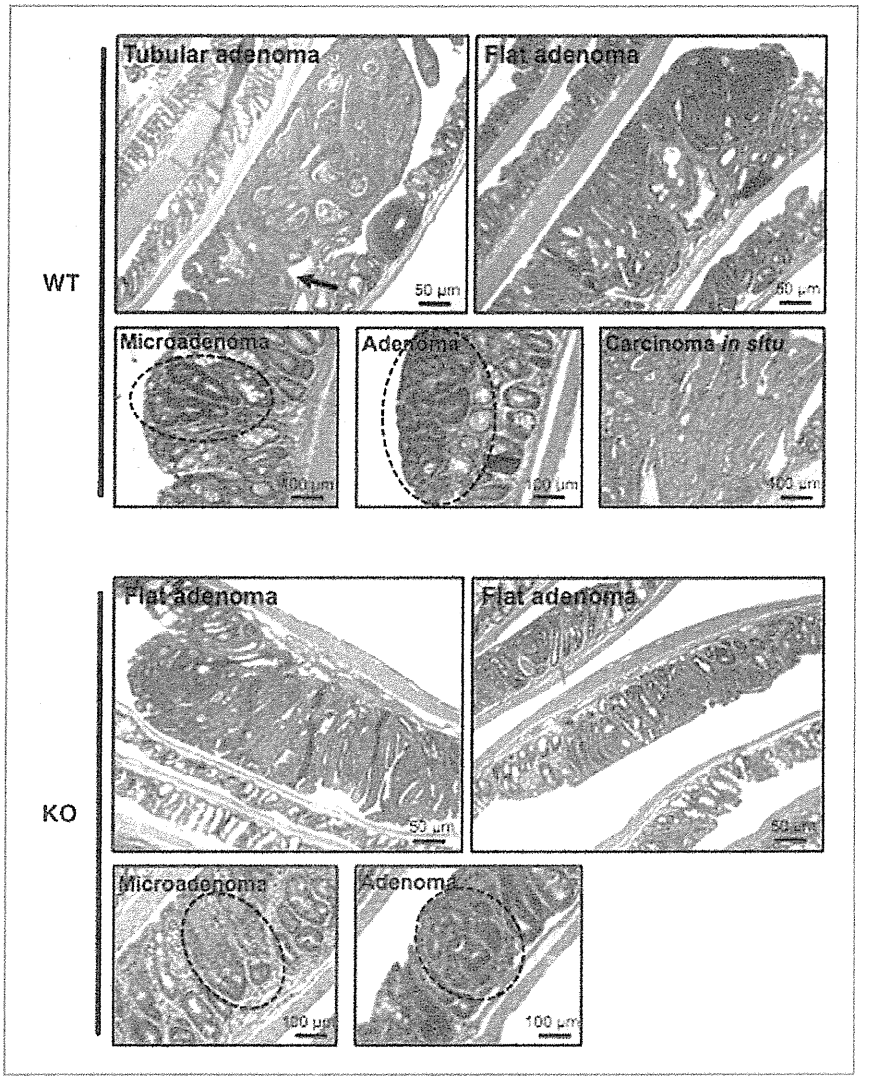

Figure 2. Evaluation of colonic lesions. Tumors in WT mice exhibit tubular or flat adenoma, whereas *mPGES-1* KO mice only develop flat or slightly raised adenomas. Microadenomas and adenomas were found in the colons of both genotypes. Carcinomas *in situ* were identified only in the WT colons. Lesions are delineated by a dotted line. $n = 14$ in WT and $n = 19$ in KO mice. Scale bars as indicated.

microadenomas showed slight, moderate, or severe nuclear atypia without evidence of expansion and invasive growth, characteristic of AOM-induced tumors occurring in this model (refs. 7, 12; Fig. 2). The morphology of the adenomas was similar between genotypes, comprised largely of microscopically tubular structures. However, tumors in WT mice were considerably larger, with frequent compression of surrounding normal crypts. In several cases, there was evidence for moderately differentiated tubular carcinomas *in situ* with invasive growth (Fig. 2, WT). Analysis of crypt dynamics revealed that within the normal colonic epithelium, the absence of *mPGES-1* did not affect overall crypt length, nor alter the size of the proliferative compartment in comparison to the WT colons (Supplementary Fig. S1).

mPGES-1 status does not affect tumor markers

The profound suppression in tumor growth observed in the *mPGES-1* KO mice raised the possibility that PGE_2 levels may directly affect cell turnover within the tumor epithelium. To evaluate this possibility, colon tumors were examined immunohistochemically for PCNA staining (proliferation), and cleaved caspase-3, which detects an earlier stage of apoptosis in cells that have not yet undergone major morphologic changes (14). A total of 10 colons from each genotype were selected for immunohistochemical analyses. Representative adenomas from a WT and *mPGES-1* KO colon are shown in Figure 3A. Intense PCNA staining was present throughout the tumor epithelium, regardless of *mPGES-1* genotype and independent of tumor size (Fig. 3A, PCNA). Cleaved caspase-3 immunostaining

Published OnlineFirst May 16, 2011; DOI:10.1158/1940-6207.CAPR-11-0188

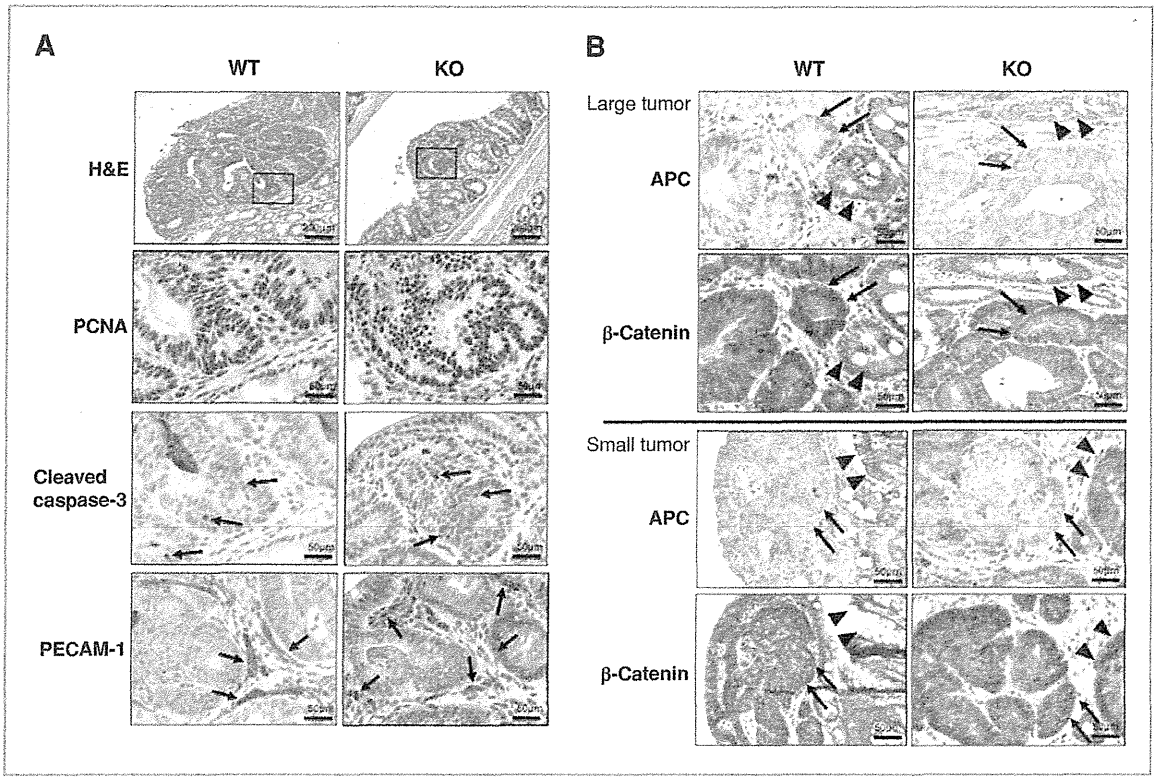

Figure 3. Immunohistochemical analysis of colon tumor markers. A, representative serial sections of colons showing staining for PCNA, cleaved caspase-3, and PECAM-1, where positive staining is indicated by the arrows. Boxed areas in H&E sections were enlarged to show the positive staining. Scale bars as indicated. B, representative images of large and small tumors from each genotype stained for APC and β-catenin. Tumor cells from either genotype lack expression of APC (arrows) compared with adjacent normal crypts (arrowheads), independent of tumor size. Similarly, β-catenin staining is increased in the tumor cells (arrows) compared with adjacent normal cells (arrowheads), independent of genotype or tumor size. $n = 10$ per group. Scale bars as indicated.

revealed few apoptotic cells within the normal crypts (data not shown), and their frequency was unaffected by *mPGES-1* status, nor affected by tumor size (Fig. 3A, cleaved caspase-3). These observations suggest that *mPGES-1* status does not influence cell turnover in the AOM colon tumor model.

In contrast to our previous findings, whereby deletion of *mPGES-1* was found to disrupt neovessel growth within small intestinal tumors in $Apc^{\Delta 14/+}$ mice (4), *mPGES-1* deletion did not directly affect PECAM-1 staining within and adjacent to AOM-induced colon tumors (Fig. 3A, PECAM-1). Even in the smallest colon lesions examined in the *mPGES-1* KO mice, PECAM-1 staining within the tumor stroma and surrounding colonic mucosa showed the presence of well-formed vascular structures (arrows; Fig. 3A, PECAM-1). The difference in PECAM-1 staining between these 2 studies, however, may result from the dissimilar experimental systems employed including differing genetic backgrounds and distinct mechanisms of tumor initiation.

We next examined the possibility that disruption of PGE_2 formation may directly impact Wnt signaling, an effect that was shown earlier in adenomatous polyposis coli (APC)-deficient DLD-1 colon cancer cells (15). Surprisingly, loss of APC protein, with increased cytoplasmic staining and nuclear localization of β-catenin, was equivalent within tumors regardless of *mPGES-1* genotype or tumor size (Fig. 3B). The loss of APC protein is consistent with previous findings showing that AOM-induced tumors do not express the full-length protein (16, 17). Taken together, these data suggest that the cancer suppression associated with reduced PGE_2 formation is not related to aberrant cell turnover or dysregulated β-catenin signaling in transformed epithelial cells.

mPGES-1 is expressed in the stroma in the colon

To define the localization of mPGES-1, immunofluorescence imaging was done on colonic mucosa prepared from mice harboring tumors. In the WT colons, we identified increased expression of mPGES-1 localized primarily at the apical surface of the tumor stroma (Fig. 4). Positive staining was also found within the stroma immediately adjacent to the tumors (ref. 18; Fig. 4, arrows). Similar to

Published OnlineFirst May 16, 2011; DOI:10.1158/1940-6207.CAPR-11-0188

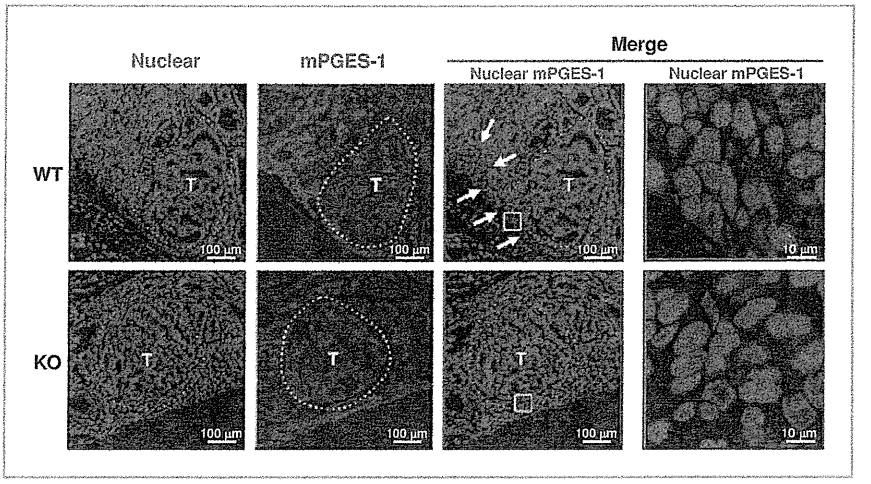

Figure 4. Immunolocalization of mPGES-1 in tumor stroma. Immunofluorescence detection of mPGES-1 in tumor and adjacent normal colonic mucosa after AOM exposure. T identifies tumor area (delineated by dotted line). Arrows in the merged images indicate the presence of mPGES-1–expressing cells at the apical surface of the tumor and also within the adjacent tumor stroma in WT mice. mPGES-1 was localized to the perinuclear region of stromal cells abutting the tumor. Scale bars as indicated.

that reported by Murakami and colleagues (19), mPGES-1 staining was confined to the perinuclear region of the cells (Fig. 4). In addition, the expression of mPGES-1 was observed within multiple cell types including macrophages and fibroblasts (ref. 20; Supplementary Fig. S2). The location of mPGES-1 indicates that the primary source of inducible PGE_2 originates within the tumor stroma (21). Therefore, an alternative possibility for tumor suppression is that genetic deletion of *mPGES-1* interrupts localized production of PGE_2 within the tumor stroma, eliciting effects that extend into the epithelial compartment.

The presence of mucosal ulcerations in *mPGES-1* KO mice

Further evaluation of colon histology in the *mPGES-1* KO mice revealed the presence of synchronous, localized mucosal ulcerations affecting up to 15% of the colonic epithelium. These cryptal lesions developed independently of AOM treatment and were characterized histologically by the presence of regenerative atypia (Fig. 5A). Mucosal ulcerations within crypt abscesses resembled the active phase of ulcerative colitis. Regenerative crypts adjacent to the ulcerated areas, as well as infiltrating immune cells, were positive for Ki-67, indicating active cell proliferation (Fig. 5A, Ki-67). However, these regenerative crypts did not share other molecular features typically associated with neoplasia. For example, APC expression was largely retained compared with the extensive loss of APC protein observed in dysplastic adenomatous crypts in the *mPGES-1* KO mice (Fig. 5B, APC). Importantly, we found no evidence for β-catenin activation within these regenerative crypt lesions, with plasma membrane staining observed in all cases examined (Fig. 5B, β-catenin). Although cyclinD1, a key β-catenin target, showed intermittent nuclear staining within these epithelial structures (Fig. 5B, cyclinD1), the normal status of APC expression and β-catenin localization within these colonic structures support their nonneoplastic nature.

Reduced frequency of $CD4^+FoxP3^+$ Tregs in the draining MLNs of the *mPGES-1* null mice

The mild and localized chronic inflammation observed within the colons of *mPGES-1* KO mice was further substantiated by the presence of macroscopically inflamed MLNs, with a significant expansion of total lymphocytes (1.6 ± 0.3 vs. 7.4 ± 1.5 in WT and KO, respectively; $P < 0.006$; Fig. 6A). Total numbers of $CD4^+$ and $CD8^+$ cells were also markedly elevated (0.9 ± 0.2 vs. 2.9 ± 0.5 for $CD4^+$ in WT and KO, respectively; $P < 0.004$ and 0.2 ± 0.04 vs. 0.8 ± 0.2 for $CD8^+$ in WT and KO, respectively; $P < 0.01$, respectively; Fig. 6A), presumably a direct result of the ongoing localized inflammation. In the spleen, however, there were no significant differences in the total numbers of both $CD4^+$ and $CD8^+$ cells (Fig. 6A). Correspondingly, serum PGE_2 concentrations were moderately ($P < 0.05$) lower in the *mPGES-1* KO than in WT mice (Supplementary Fig. S3A). Moreover, the concentration of a panel of pro- and anti-inflammatory cytokines in the serum was mostly unchanged between genotypes, confirming the localized effect associated with *mPGES-1* deletion (Supplementary Fig. S3B). The only exception was a significant decrease in IL-1α in *mPGES-1* KO mice, which was recently shown to be regulated by PGE_2 (22) and might be indicative of a stronger chronic inflammatory response.

We next investigated the immunoregulatory mechanisms that may underlie colonic inflammation in the *mPGES-1* KO mice. PGE_2 has been shown *in vitro* to enhance the differentiation of naive $CD4^+$ T cells into FoxP3-positive Tregs that have the potential to suppress effector T-cell function (23). Furthermore, Tregs play an important regulatory role in gastrointestinal immunity (24). As shown in Figure 6B, in the MLNs of *mPGES-1* KO mice, the frequency of CD4 FoxP3 double-positive cells was reduced by 55% compared than in WT mice (21.1 ± 1.1 vs. 11.7 ± 1.3 in WT and KO, respectively; $P < 0.0004$). Importantly, this effect was not systemic, as

Published OnlineFirst May 16, 2011; DOI:10.1158/1940-6207.CAPR-11-0188

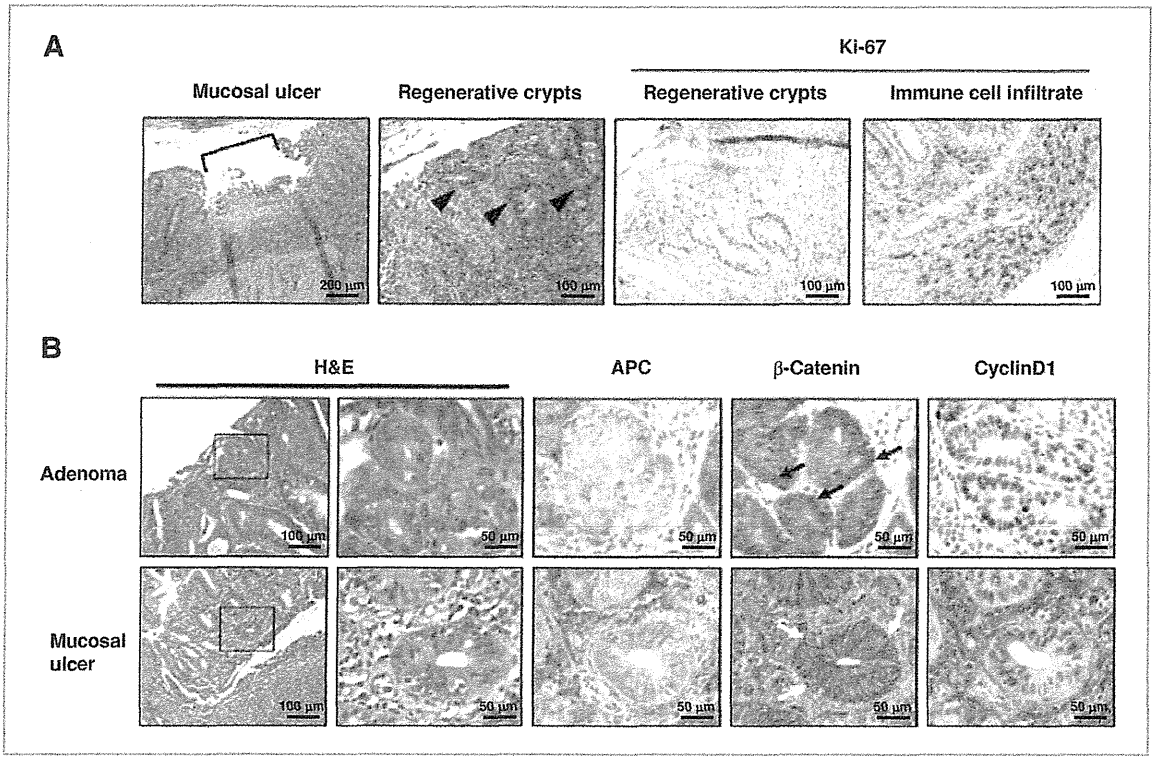

Figure 5. Histologic features of localized colonic ulcerations. A, a representative localized ulceration in the colon of a *mPGES-1* KO mouse containing regenerative crypts (arrowheads). Highly proliferative cells within the regenerative crypts are detected by Ki-67 staining. Intense Ki-67 staining is also seen in infiltrating immune cells within the colonic mucosa. B, comparison of tumor-related markers in serial sections of tumors and mucosal ulcers in *mPGES-1* KO mice. Enlarged areas are identified by the box. Scale bars as indicated.

the composition of Tregs within the spleen was unaffected by genotype (Fig. 6B).

We also examined the possibility that a population of myeloid-derived suppressor cells (MDSC), immunomodulatory cells that are often increased in tumor-bearing mice (25), may be expanded in *mPGES-1* KO mice in response to the localized mucosal ulcerations. As anticipated, increased levels of GR-1 CD11b double-positive MDSCs were found in the MLN (0.03 ± 0.02 vs. 0.20 ± 0.03 in WT and KO, respectively; $P < 0.00004$) and spleen (2.08 ± 0.40 vs. 8.37 ± 2.76 in WT and KO, respectively; $P < 0.01$; Fig. 6C). However, the frequency of MDSCs was modest in comparison to changes found in other mouse tumor models. For example, in some cases, the spleen can harbor up to 40% of MDSCs within the T-cell population, depending of course on the underlying pathology (26). The present findings suggest that limited expansion of MDSCs in *mPGES-1* KO mice, most likely attributed to reduced PGE_2 levels (27), contributes to the enhanced inflammatory state that is present within the colon and that may ultimately impede colon tumor progression.

On the basis of the reduced levels of Tregs and the moderate effect on MDSCs, we postulated that additional immunoregulatory mechanisms might also contribute to tumor suppression. Thus to evaluate this possibility, we harvested cells from the spleens and MLNs of untreated WT and *mPGES-1* KO mice. The total number of cells harvested from the MLN of the *mPGES-1* KO mice was significantly higher in comparison to the WT mice, a result of the localized colonic ulcerations (Supplementary Fig. S4). In addition, the number of $CD4^+$ and $CD8^+$ cells was also markedly higher in the *mPGES-1* KO MLN (Supplementary Fig. S4), consistent with our findings in tumor-bearing mice (Fig. 6A). Following a 4-hour stimulation with PMA/ionomycin, the ability of $CD4^+$ cells to produce IL-10 or IFN-γ was slightly impaired in the *mPGES-1* KO group (Supplementary Fig. S4). These observations suggest that *mPGES-1* deficiency may affect the production of regulatory T type 1 cells (Tr1), another type of immunoregulatory cell present within the gut mucosa (28).

Discussion

Elevated prostanoid production in the colon plays a key role in cancer pathogenesis and efforts have been made to suppress this pathway, primarily via inhibition

Published OnlineFirst May 16, 2011; DOI:10.1158/1940-6207.CAPR-11-0188

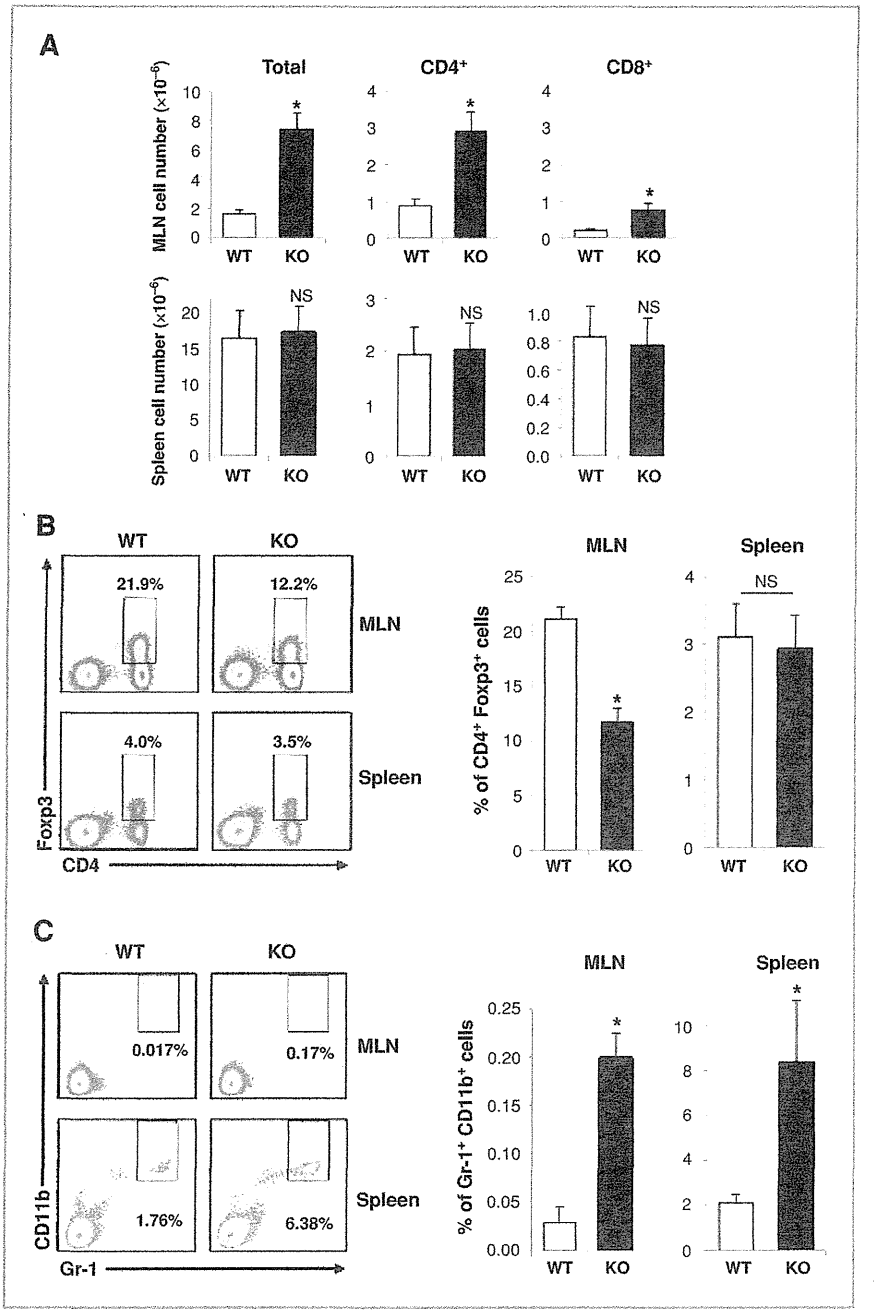

Figure 6. Flow cytometry of cells in MLNs and spleens. A, total numbers of cells in MLN and spleen, including the number of $CD4^+$ and $CD8^+$ T cells. B, representative FACS analysis showing the frequency of CD4 FoxP3 double-positive Tregs. Quantification of FACS analyses is expressed as means ± SEM, $n = 9$ per group. C, representative FACS analysis showing frequency of Gr-1 CD11b double-positive MDSCs. Quantification of FACS analysis is expressed as means ± SEM, $n = 8$ in WT and $n = 6$ in KO mice. *, $P < 0.05$; NS, not significant compared with WT mice.

of COX-2 activity. Although long-term COX-2 inhibition can be effective, it has also been associated with a number of adverse effects, notably cardiovascular and gastrointestinal (GI) toxicities (29). Evidence from several tumor models provides the rationale for the development of alternative chemoprevention targets within the arachidonic acid pathway including the terminal PGE_2 synthase, mPGES-1 (3). In the present study, we provide evidence that suppression of inducible PGE_2 production through genetic deletion of *mPGES-1* effectively reduces colon cancer development. We also go on to show that suppressing inducible PGE_2 formation

Published OnlineFirst May 16, 2011; DOI:10.1158/1940-6207.CAPR-11-0188

influences cancer development in part by promoting an effective immune response to the tumor.

Remarkably, tumor suppression was so effective that only 1 of 19 *mPGES-1* KO mice (5.3%) developed a colon tumor exceeding 3 mm in size. Despite this protection afforded to the colon, however, *mPGES-1* deletion did not influence the frequency of ACF to the same extent. This latter observation is consistent with the recent findings of Cho and colleagues (30) who reported that within a subset of patients on the Adenoma Prevention with Celecoxib trial, adenoma suppression by celecoxib treatment was not correlated with changes in the density of ACF within the distal colorectum. It is possible that at least for agents that target the COX-2 pathway, ACF do not provide a surrogate marker for colon cancer suppression.

PGE_2 is a pleiotropic molecule that is formed within a variety of cell types and can elicit effects that are both cell- and tissue-context dependent. The precise location of inducible PGE_2 formation, however, remains somewhat controversial. For example, it is broadly accepted that tumor cell–derived PGE_2 promotes tumor growth through an autocrine mechanism. Consistent with this mechanism, mPGES-1 expression has been identified directly within the epithelial cells of colon tumors (31–33). In the present study, however, we found that mPGES-1 was localized primarily within the tumor stroma, indicating that inducible formation of PGE_2 may impair tumor expansion via non–cell autonomous mechanisms. This finding is consistent with the results of Kamei and colleagues (32), who showed that the growth of Lewis lung carcinoma (LLC) tumor cells explanted into an *mPGES-1*–deficient host was markedly impaired in comparison to the growth observed in an *mPGES-1*–competent host. In addition, a number of studies have found COX-2 expression to be confined to the tumor stroma (reviewed in ref. 34).

The depletion of inducible PGE_2 formation is associated with the development of colonic mucosal abnormalities that are reminiscent of ulcerative colitis. The lesions are restricted to the large intestine, and the histologic features of these lesions consist of crypt erosion and an influx of inflammatory cells. Interestingly, Hara and colleagues (35) recently reported that *mPGES-1* KO mice show enhanced susceptibility to dextran sodium sulfate (DSS)-induced ulcerative colitis, confirming a critical role for PGE_2 in maintaining colonic epithelial barrier function under conditions of chemical-induced stress. It is possible that the localized ulcerations present within the colons of the *mPGES-1* KO mice induce a chronic inflammatory condition. We further speculate that this underlying inflammation may actually be a contributing factor in the suppression of colon tumors observed in the present study.

PGE_2 is among the most potent immunoregulatory molecules within the intestinal mucosa. In addition to its modulating effects on normal gut barrier function and mucosal response to pathogens (36), inducible formation of PGE_2 also plays a critical role in the immunosuppression associated with advanced neoplasia (37). Tregs, with the potential to suppress effector T-cell function (38, 39) have been shown to play an important immunomodulatory role within the GI tract (24, 40). Within the tumor microenvironment, PGE_2 has been reported to enhance Treg differentiation by inducing the expression of Foxp3 in naive $CD4^+$ T cells (23, 41, 42). In CRC patients, increased levels of Tregs were identified within the tumors as well as in the regional lymph nodes (43). Moreover, the effect of Tregs on the production of proinflammatory cytokines was reversed by treatment with nonsteroidal anti-inflammatory drugs (NSAID), further evidence for Treg dependence on PGE_2 during tumor evolution (43). Given the direct influence that PGE_2 elicits on FoxP3 expression in T cells, it is entirely possible that *mPGES-1* deficiency may result in a persistent overreactive immune response due to the loss of functional activation of Tregs.

Interestingly, the present study shows that the impaired immunoregulatory response in the *mPGES-1* KO mice, reflected by the spontaneous development of localized ulcerations, was not entirely accounted for by attenuated Treg expansion. *mPGES-1* deletion also modestly affected the levels of MDSCs and Tr1-like cells, suggesting that the absence of inducible PGE_2 formation may disrupt fundamental immunomodulatory mechanisms within the tumor microenvironment. One possibility is that *mPGES-1* deficiency causes a shift in cytokine profiles during tumorigenesis. In fact, Monrad and colleagues (44) recently showed that *mPGES-1*–deficient bone marrow–derived dendritic cells (BMDC) had decreased production of IL-12 in response to lipopolysaccharide (LPS) stimulation. Furthermore, our preliminary data show that MLN cells harvested from the *mPGES-1* KO mice produce higher levels of several cytokines when compared with similarly stimulated WT cells (data not shown). Because the *mPGES-1* genotype did not affect systemic cytokine profiles with the exception of IL-1α, a more detailed analysis of tissue-specific cytokine profiles is warranted.

A number of studies suggest that chronic inflammation may play an important role in the pathogenesis of up to 20% of human cancers (45). In particular, long-standing inflammatory bowel disease (IBD) is considered a significant risk factor for CRC (46). Although the present data appear to contradict these earlier observations, we postulate that the underlying inflammation present in *mPGES-1* KO mice, resulting from the mild and localized colonic ulceration, may actually confer protection against tumor progression by providing a mechanism for active clearance of cancer-initiating cells. Consistent with this hypothesis, an earlier study by Tanaka and colleagues (13) showed that mice administered DSS prior to a single injection of AOM failed to develop colon tumors 20 weeks later. In the present study, *mPGES-1* KO mice did not exhibit clinical signs of severe ulcerative colitis, such as rectal bleeding and excessive weight loss (data not shown), despite the presence of these benign, localized mucosal ulcerations. Of course, the possibility exists that the mild inflammation that is present within the colons

Published OnlineFirst May 16, 2011; DOI:10.1158/1940-6207.CAPR-11-0188

of the *mPGES-1* KO mice may contribute to subsequent cancer risk. However, without additional genetic hits, these lesions may not have the capacity to progress to cancer (47). Therefore, additional studies to better define the mechanisms by which selective suppression of PGE_2 directly modulates antitumor immunity and contributes to colon cancer suppression are underway. These studies will ultimately enable the development of effective therapeutic strategies for targeting mPGES-1 for cancer prevention.

Disclosure of Potential Conflicts of Interest

No potential conflicts of interest were disclosed.

Acknowledgment

The authors thank Dr. Robert Clark in Department of Immunology at University of Connecticut Health Center for his advice on designing experiments for Treg analyses.

Grant Support

This work was supported by NIH grant CA-125691 and CA-114635 (D.W. Rosenberg).

The costs of publication of this article were defrayed in part by the payment of page charges. This article must therefore be hereby marked *advertisement* in accordance with 18 U.S.C. Section 1734 solely to indicate this fact.

Received April 11, 2011; revised May 5, 2011; accepted May 6, 2011; published OnlineFirst May 19, 2011.

References

1. Radmark O, Samuelsson B. Microsomal prostaglandin E synthase-1 and 5-lipoxygenase: potential drug targets in cancer. J Intern Med 2010;268:5–14.
2. Samuelsson B, Morgenstern R, Jakobsson PJ. Membrane prostaglandin E synthase-1: a novel therapeutic target. Pharmacol Rev 2007;59:207–24.
3. Nakanishi M, Gokhale V, Meuillet EJ, Rosenberg DW. mPGES-1 as a target for cancer suppression: a comprehensive invited review "Phospholipase A2 and lipid mediators". Biochimie 2010;92:660–4.
4. Nakanishi M, Montrose DC, Clark P, Nambiar PR, Belinsky GS, Claffey KP, et al. Genetic deletion of mPGES-1 suppresses intestinal tumorigenesis. Cancer Res 2008;68:3251–9.
5. Moser AR, Luongo C, Gould KA, McNeley MK, Shoemaker AR, Dove WF. ApcMin: a mouse model for intestinal and mammary tumorigenesis. Eur J Cancer 1995;31A:1061–4.
6. Nambiar PR, Nakanishi M, Gupta R, Cheung E, Firouzi A, Ma XJ, et al. Genetic signatures of high- and low-risk aberrant crypt foci in a mouse model of sporadic colon cancer. Cancer Res 2004;64:6394–401.
7. Papanikolaou A, Wang QS, Papanikolaou D, Whiteley HE, Rosenberg DW. Sequential and morphological analyses of aberrant crypt foci formation in mice of differing susceptibility to azoxymethane-induced colon carcinogenesis. Carcinogenesis 2000;21:1567–72.
8. Rosenberg DW, Giardina C, Tanaka T. Mouse models for the study of colon carcinogenesis. Carcinogenesis 2009;30:183–96.
9. Uematsu S, Matsumoto M, Takeda K, Akira S. Lipopolysaccharide-dependent prostaglandin E(2) production is regulated by the glutathione-dependent prostaglandin E(2) synthase gene induced by the Toll-like receptor 4/MyD88/NF-IL6 pathway. J Immunol 2002; 168:5811–6.
10. Unkeless JC, Kaplan G, Plutner H, Cohn ZA. Fc-receptor variants of a mouse macrophage cell line. Proc Natl Acad Sci U S A 1979;76:1400–4.
11. Menoret A, Myers LM, Lee SJ, Mittler RS, Rossi RJ, Vella AT. TGFbeta protein processing and activity through TCR triggering of primary $CD8^+$ T regulatory cells. J Immunol 2006;177:6091–7.
12. Nambiar PR, Nakanishi M, Gupta RA, Cheung E, Firouzi A, Ma XJ, et al. Molecular signatures of high and low risk aberrant crypt foci in a mouse model of sporadic colon cancer. Dig Dis Week 2004:501.
13. Tanaka T, Kohno H, Suzuki R, Yamada Y, Sugie S, Mori H. A novel inflammation-related mouse colon carcinogenesis model induced by azoxymethane and dextran sodium sulfate. Cancer Sci 2003;94: 965–73.
14. Greenspan EJ, Nichols FC, Rosenberg DW. Molecular alterations associated with sulindac-resistant colon tumors in $ApcMin/^+$ mice. Cancer Prev Res 2010;3:1187–97.
15. Castellone MD, Teramoto H, Williams BO, Druey KM, Gutkind JS. Prostaglandin E2 promotes colon cancer cell growth through a Gs-axin-beta-catenin signaling axis. Science 2005;310:1504–10.
16. Guda K, Upender MB, Belinsky G, Flynn C, Nakanishi M, Marino JN, et al. Carcinogen-induced colon tumors in mice are chromosomally stable and are characterized by low-level microsatellite instability. Oncogene 2004;23:3813–21.
17. Maltzman T, Whittington J, Driggers L, Stephens J, Ahnen D. AOM-induced mouse colon tumors do not express full-length APC protein. Carcinogenesis 1997;18:2435–9.
18. Takeda H, Sonoshita M, Oshima H, Sugihara K, Chulada PC, Langenbach R, et al. Cooperation of cyclooxygenase 1 and cyclooxygenase 2 in intestinal polyposis. Cancer Res 2003;63:4872–7.
19. Murakami M, Naraba H, Tanioka T, Semmyo N, Nakatani Y, Kojima F, et al. Regulation of prostaglandin E2 biosynthesis by inducible membrane-associated prostaglandin E2 synthase that acts in concert with cyclooxygenase-2. J Biol Chem 2000;275:32783–92.
20. Gudis K, Tatsuguchi A, Wada K, Futagami S, Nagata K, Hiratsuka T, et al. Microsomal prostaglandin E synthase (mPGES)-1, mPGES-2 and cytosolic PGES expression in human gastritis and gastric ulcer tissue. Lab Invest 2005;85:225–36.
21. Backlund MG, Mann JR, Dubois RN. Mechanisms for the prevention of gastrointestinal cancer: the role of prostaglandin E2. Oncology 2005;69 Suppl 1:28–32.
22. Shao J, Sheng H. Prostaglandin E2 induces the expression of IL-1alpha in colon cancer cells. J Immunol 2007;178:4097–103.
23. Sharma S, Yang SC, Zhu L, Reckamp K, Gardner B, Baratelli F, et al. Tumor cyclooxygenase-2/prostaglandin E2-dependent promotion of FOXP3 expression and $CD4^+$ $CD25^+$ T regulatory cell activities in lung cancer. Cancer Res 2005;65:5211–20.
24. Read S, Malmstrom V, Powrie F. Cytotoxic T lymphocyte-associated antigen 4 plays an essential role in the function of CD25(+)CD4(+) regulatory cells that control intestinal inflammation. J Exp Med 2000;192:295–302.
25. Ostrand-Rosenberg S, Sinha P. Myeloid-derived suppressor cells: linking inflammation and cancer. J Immunol 2009;182:4499–506.
26. Gabrilovich DI, Nagaraj S. Myeloid-derived suppressor cells as regulators of the immune system. Nat Rev Immunol 2009;9:162–74.
27. Sinha P, Clements VK, Fulton AM, Ostrand-Rosenberg S. Prostaglandin E2 promotes tumor progression by inducing myeloid-derived suppressor cells. Cancer Res 2007;67:4507–13.
28. Vieira PL, Christensen JR, Minaee S, O'Neill EJ, Barrat FJ, Boonstra A, et al. IL-10-secreting regulatory T cells do not express Foxp3 but have comparable regulatory function to naturally occurring $CD4^+CD25^+$ regulatory T cells. J Immunol 2004;172:5986–93.
29. Wang D, Dubois RN. The role of COX-2 in intestinal inflammation and colorectal cancer. Oncogene 2010;29:781–8.
30. Cho NL, Redston M, Zauber AG, Carothers AM, Hornick J, Wilton A, et al. Aberrant crypt foci in the adenoma prevention with celecoxib trial. Cancer Prev Res 2008;1:21–31.
31. Golijanin D, Tan JY, Kazior A, Cohen EG, Russo P, Dalbagni G, et al. Cyclooxygenase-2 and microsomal prostaglandin E synthase-1 are overexpressed in squamous cell carcinoma of the penis. Clin Cancer Res 2004;10:1024–31.

Published OnlineFirst May 16, 2011; DOI:10.1158/1940-6207.CAPR-11-0188

32. Kamei D, Murakami M, Sasaki Y, Nakatani Y, Majima M, Ishikawa Y, et al. Microsomal prostaglandin E synthase-1 in both cancer cells and hosts contributes to tumour growth, invasion and metastasis. Biochem J 2009;425:361–71.
33. Yoshimatsu K, Golijanin D, Paty PB, Soslow RA, Jakobsson PJ, DeLellis RA, et al. Inducible microsomal prostaglandin E synthase is overexpressed in colorectal adenomas and cancer. Clin Cancer Res 2001;7:3971–6.
34. Williams CS, DuBois RN. Prostaglandin endoperoxide synthase: why two isoforms? Am J Physiol 1996;270:G393–400.
35. Hara S, Kamei D, Sasaki Y, Tanemoto A, Nakatani Y, Murakami M. Prostaglandin E synthases: understanding their pathophysiological roles through mouse genetic models. Biochimie 2010;92:651–9.
36. Montrose DC, Kadaveru K, Ilsley JN, Root SH, Rajan TV, Ramesh M, et al. cPLA2 is protective against COX inhibitor-induced intestinal damage. Toxicol Sci 2010;117:122–32.
37. Tilley SL, Coffman TM, Koller BH. Mixed messages: modulation of inflammation and immune responses by prostaglandins and thromboxanes. J Clin Invest 2001;108:15–23.
38. Sakaguchi S, Sakaguchi N, Asano M, Itoh M, Toda M. Immunologic self-tolerance maintained by activated T cells expressing IL-2 receptor alpha-chains (CD25). Breakdown of a single mechanism of self-tolerance causes various autoimmune diseases. J Immunol 1995;155:1151–64.
39. Seddon B, Mason D. Regulatory T cells in the control of autoimmunity: the essential role of transforming growth factor beta and interleukin 4 in the prevention of autoimmune thyroiditis in rats by peripheral CD4(+)CD45RC- cells and CD4(+)CD8(-) thymocytes. J Exp Med 1999;189:279–88.
40. Maloy KJ, Salaun L, Cahill R, Dougan G, Saunders NJ, Powrie F. $CD4^+CD25^+$ T(R) cells suppress innate immune pathology through cytokine-dependent mechanisms. J Exp Med 2003;197:111–9.
41. Mahic M, Yaqub S, Johansson CC, Tasken K, Aandahl EM. $FOXP3^+CD4^+CD25^+$ adaptive regulatory T cells express cyclooxygenase-2 and suppress effector T cells by a prostaglandin E2-dependent mechanism. J Immunol 2006;177:246–54.
42. Baratelli F, Lin Y, Zhu L, Yang SC, Heuzé-Vourc'h N, Zeng G, et al. Prostaglandin E2 induces FOXP3 gene expression and T regulatory cell function in human $CD4^+$ T cells. J Immunol 2005;175:1483–90.
43. Yaqub S, Henjum K, Mahic M, Jahnsen FL, Aandahl EM, Bjørnbeth BA, et al. Regulatory T cells in colorectal cancer patients suppress anti-tumor immune activity in a COX-2 dependent manner. Cancer Immunol Immunother 2008;57:813–21.
44. Monrad SU, Kojima F, Kapoor M, Kuan EL, Sarkar S, Randolph GJ, et al. Genetic deletion of mPGES-1 abolishes PGE2 production in murine dendritic cells and alters the cytokine profile, but does not affect maturation or migration. Prostaglandins Leukot Essent Fatty Acids 2011;84:113–21.
45. Aggarwal BB, Vijayalekshmi RV, Sung B. Targeting inflammatory pathways for prevention and therapy of cancer: short-term friend, long-term foe. Clin Cancer Res 2009;15:425–30.
46. Waldner MJ, Neurath MF. Colitis-associated cancer: the role of T cells in tumor development. Semin Immunopathol 2009;31:249–56.
47. Mladenova D, Daniel JJ, Dahlstrom JE, Bean E, Gupta R, Pickford R, et al. The NSAID sulindac is chemopreventive in the mouse distal colon but carcinogenic in the proximal colon. Gut 2011;60:350–60.

72-79
Nutrition and Cancer, 63:8, 2011

ISSN: 0163-5581 print / 1532-7914 online
DOI: 10.1080/01635581.2012.630554

Routledge
Taylor & Francis Group

Preventive Effects of Curcumin on the Development of Azoxymethane-Induced Colonic Preneoplastic Lesions in Male C57BL/KsJ-*db/db* Obese Mice

Masaya Kubota, Masahito Shimizu, Hiroyasu Sakai, Yoichi Yasuda, Daishi Terakura, Atsushi Baba, Tomohiko Ohno, and Hisashi Tsurumi
Department of Internal Medicine, Gifu University Graduate School of Medicine, Gifu, Japan

Takuji Tanaka
Department of Oncologic Pathology, Kanazawa Medical University, Ishikawa, Japan

Hisataka Moriwaki
Department of Internal Medicine, Gifu University Graduate School of Medicine, Gifu, Japan

Obesity-related metabolic abnormalities include a state of chronic inflammation and adipocytokine imbalance, which increase the risk of colon cancer. Curcumin, a component of turmeric, exerts both cancer preventive and antiinflammatory properties. Curcumin is also expected to have the ability to reverse obesity-related metabolic derangements. The present study examined the effects of curcumin on the development of azoxymethane (AOM)-induced colonic premalignant lesions in C57BL/KsJ-*db/db* (*db/db*) obese mice. Feeding with a diet containing 0.2% and 2.0% curcumin caused a significant reduction in the total number of colonic premalignant lesions compared with basal diet-fed mice. The expression levels of tumor necrosis factor-α, interleukin-6, and cyclooxygenase-2 (COX-2) mRNAs on the colonic mucosa of AOM-treated mice were significantly decreased by curcumin administration. Dietary feeding with curcumin markedly activated AMP-activated kinase, decreased the expression of COX-2 protein, and inhibited nuclear factor-κB activity on the colonic mucosa of AOM-treated mice. Curcumin also increased the serum levels of adiponectin while conversely decreasing the serum levels of leptin and the weights of fat. In conclusion, curcumin inhibits the development of colonic premalignant lesions in an obesity-related colorectal carcinogenesis model, at least in part, by attenuating chronic inflammation and improving adipocytokine imbalance. Curcumin may be useful in the chemoprevention of colorectal carcinogenesis in obese individuals.

Submitted 28 June 2010; accepted in final form 20 June 2011.
Address correspondence to Masahito Shimizu, Department of Internal Medicine, Gifu University Graduate School of Medicine, 1-1 Yanagido, Gifu 501-1194, Japan. Phone: +81-(58) 230-6313. Fax: +81-(58) 230-6310. E-mail: shimim-gif@umin.ac.jp

INTRODUCTION

Colorectal cancer (CRC) is a serious global health care problem. There is increasing evidence that obesity and its related metabolic abnormalities are associated with colorectal carcinogenesis. Several biological mechanisms linking obesity to the development of CRC have been demonstrated, including the emergence of insulin resistance and alterations in the insulin-like growth factor (IGF)/IGF-1 receptor axis (1,2). Imbalance of adipocytokines (such as decreased adiponectin levels and increased leptin levels) and a state of chronic inflammation, both of which are highly correlated with the presence of excess adipose tissue, also play roles in obesity-related colorectal carcinogenesis (1,2). For instance, there is a close correlation between lower levels of serum adiponectin and the development of colorectal tumors (3,4). Increased leptin levels exert tumor-promoting effects in obesity- and inflammation-related CRC (5–9). Tumor necrosis factor (TNF)-α, a central mediator of chronic inflammatory diseases, has markedly increased expression levels in adipose tissue, and its dysregulation is associated with stimulation of tumor promotion and progression of carcinogenesis (10,11). These reports suggest that targeting adipocytokine imbalance and chronic inflammation may provide effective strategies for preventing the development of obesity-related CRC (6–8).

Curcumin, a yellow-colored pigment derived from turmeric (Curcuma longa), has been shown to exert numerous pharmacological effects, including antiinflammatory and chemopreventive properties (12–14). In rodent models, dietary curcumin was found to inhibit chemically induced colorectal carcinogenesis (see the Chemopreventive Database at http://www.inra.fr/reseau-nacre/sci-memb/corpet/indexan.html). Curcumin also inhibited cell growth and induced apoptosis in human CRC-derived cells

by suppressing the expression of cyclooxygenase-2 (COX-2) (15,16), which is one of the most critical targets of CRC chemoprevention (17). Curcumin showed benefits in the treatment of ulcerative colitis in a randomized clinical trial (18), and it was also found to attenuate chronic experimental colitis in rats by reducing the expression of TNF-α and COX-2 on the colonic mucosa (19). Therefore, curcumin may be capable of exerting chemopreventive and antiinflammatory effects on the colon through regulation of TNF-α and COX-2 expression.

In addition, recent studies have revealed that curcumin has the potential to improve obesity-related chronic inflammatory conditions and metabolic derangements. In rodent models of obesity and diabetes, administration of curcumin significantly ameliorates diabetes, increases adiponectin production by adipose tissue, and decreases serum levels of TNF-α and interleukin (IL)-6 (20,21). Therefore, curcumin may be a promising agent for the prevention of obesity-related pathogenesis including CRC development. In the present study, we investigated the effects of curcumin on the development of colonic premalignant lesions, aberrant crypt foci (ACF), and β-catenin accumulated crypts (BCAC) (22,23) in an animal model for obesity-related colorectal carcinogenesis (5–8), which was produced by administrating the colonic carcinogen azoxymethane (AOM) to obese and diabetic C57BL/KsJ-*db/db* (*db/db*) mice.

MATERIALS AND METHODS

Animals and Chemicals

Four-week-old male homozygous *db/db* mice were obtained from Japan SLC (Shizuoka, Japan) and were maintained at the Gifu University Life Science Research Center in accordance with the Institutional Animal Care Guidelines. Curcumin and AOM were purchased from Sigma-Aldrich (St. Louis, MO).

Experimental Procedure

A total of 38 male *db/db* mice were divided into the following 5 experimental and control groups: untreated (Group 1, $n = 5$); 2% curcumin alone (Group 2, $n = 5$); AOM alone (Group 3, $n = 10$); AOM plus 0.2% curcumin (Group 4, $n = 9$); and AOM plus 2% curcumin (Group 5, $n = 9$). The curcumin concentrations (0.2% and 2%) were chosen based on the following 2 reasons: 1) the doses of dietary curcumin in the most published rodent experiments were between 0.05 and 2% from the Chemopreventive Database; and 2) the dose level of 0.2% curcumin in diet, which is equivalent to 300mg/kg/day (24), is relevant to the dose used in clinical trials. At 5 wk of age, all mice were given 4 weekly subcutaneous injections of saline (Groups 1 and 2) or AOM (15 mg/kg body weight; Groups 3, 4, and 5). The mice in Groups 1 and 3 were fed the basal diet, CRF-1 (Oriental Yeast Co., Ltd., Tokyo, Japan), throughout the experiment (for 11 wk). Group 2 was fed the basal diet containing 2% curcumin throughout the experiment. Groups 4 and 5 were given the basal diet containing 0.2% and 2% curcumin, respectively, for 7 wk, starting 1 wk after the last injection of AOM. At the termination of the study (16 wk of age), all mice were sacrificed for analysis of ACF and BCAC. The animal experiment was approved by the Committee of the Institutional Animal Experiments of Gifu University.

Identification and Counting of ACF and BCAC

The numbers of ACF and BCAC were determined according to standard procedures (6–8). After fixing flat in 10% buffered formalin for 24 h, the colons were stained with methylene blue (0.5% in distilled water) to count the number of ACF. The distal parts of the colon (2 cm from anus; mean area, 0.7 cm^2/colon) were then cut and embedded in paraffin, and a total of 20 serial sections (each 4 μm thick) per mouse were created by an en face preparation to identify BCAC intramucosal lesions (6–8). For each case, 2 serial sections were used to analyze BCAC.

Histopathology and Immunohistochemical Analyses for β-Catenin and Nuclear Factor-κB

Two serial sections, prepared from the paraffin-embedded tissue blocks, were subjected to hematoxylin and eosin staining for histopathology and β-catenin immunohistochemistry to count the number of BCAC (6–8). In addition, phospho-nuclear factor-κB (NF-κB) p65 immunohistochemistry was performed in vertical histological sections of colonic mucosa to estimate NF-κB activity in the crypt cells and mucosal interstitial cells (25). Immunohistochemistry for β-catenin and phospho-NF-κB p65 was performed using the labeled streptavidin-biotin method (LSAB kit; DAKO, Glostrup, Denmark). Anti-β-catenin antibody (1:1000 final dilution) was obtained from BD Transduction Laboratories (San Jose, CA). Antiphospho-NF-κB p65 antibody (Ser276; 1:50 final dilution) was from Cell Signaling Technology (Danvers, MA). In the phospho-NF-κB p65-immunostained sections, the cells with intensely stained nuclei were considered to be active in NF-κB. Cells with active NF-κB in both the colonic epithelium and interstitium were counted and expressed as a percentage of the total number of cells in the tissues. A positive cell index (%) was determined by counting at least 500 cells in the colonic epithelium and 300 cells in the interstitium of each mouse.

Protein Extraction and Western Blot Analysis

Total proteins were extracted from the scraped mucosa from the remaining colon portions of the AOM-treated mice (Groups 3 to 5), and equivalent amounts of proteins (20 μg/lane) were examined by a Western blot analysis (6–8). The primary antibodies for AMP-activated kinase (AMPK), phosphorylated form of AMPK, COX-2, and glyceraldehyde-3-phosphate dehydrogenase (GAPDH) were described previously (6–8). An antibody against GAPDH served as a loading control.

RNA Extraction and Quantitative Real-Time Reverse Transcription-PCR analysis

Total RNA was isolated from the scraped colonic mucosa of the AOM-treated mice using the RNAqueous-4PCR kit

(Ambion Applied Biosystems, Austin, TX). The cDNA was synthesized from 0.2 μg of total RNA using the SuperScript III First-Strand Synthesis System (Invitrogen, San Diego, CA). A quantitative real-time reverse transcription-PCR (RT-PCR) analysis was performed using specific primers that amplify the TNF-α, IL-6, COX-2, and GAPDH genes, as previously described (8). Real-time RT-PCR was done in a LightCycler (Roche Diagnostics Co., Indianapolis, IN) with the SYBR Premix Ex Taq (TaKaRa Bio, Shiga, Japan). The expression levels of the TNF-α, IL-6, and COX-2 genes were normalized to the GAPDH gene expression levels.

Clinical Chemistry

The blood samples, which were collected at the time of sacrifice after 6 h of fasting, were used for chemical analyses. The serum concentrations of adiponectin and leptin (Shibayagi, Gunma, Japan) were determined by using an enzyme immunoassay according to the manufacturer's protocol.

Statistical Analyses

The results are presented as the mean $\pm$ SD and were analyzed using the GraphPad Instat software program, v. 3.05 (GraphPad Software, San Diego, CA) for Macintosh. The differences among the groups were analyzed by 1-way analysis of variance (ANOVA) or by 2-way ANOVA if required. When ANOVA showed a statistically significant effect ($P < 0.05$), comparison of each experimental group with the control group was performed using the Tukey-Kramer multiple comparisons test. The differences were considered statistically significant when the 2-tailed P-value was less than 0.05.

RESULTS

General Observations

During the study, dietary feeding with curcumin did not cause clinical symptoms or evidence of toxicity (data not shown). The mean body weights of the AOM-injected groups (Group 3: 40.9 $\pm$ 5.5 g, Group 4: 35.0 $\pm$ 2.6 g, and Group 5: 39.1 $\pm$ 6.1 g) were lower than that of the saline-injected group (Group 1: 54.6 $\pm$ 8.8 g) at the termination of the experiment ($P < 0.01$ for each comparison). This might be caused by the toxicity of AOM, which has been observed in previous experiments (6–8). No significant differences were observed in the mean weights of the liver and kidney among the groups (data not shown). Histopathological examination also revealed that there were no alterations visible in the liver and kidney tissues. This provides further evidence of the lack of toxicity of curcumin with respect to the liver and kidney of the mice in Groups 3 to 5 (data not shown).

Effects of Curcumin on AOM-Induced ACF and BCAC Formations in *db/db* Mice

Table 1 summarizes the total numbers of ACF and BCAC in each group. ACF and BCAC were observed to develop in the colon of all mice that received AOM (Groups 3 to 5), but not in the control groups (Groups 1 and 2). The mean number of ACF in the AOM alone group (Group 3) was 134.0 $\pm$ 24.5 and dietary feeding with 0.2% (Group 4) and 2% (Group 5) curcumin significantly reduced the incidence of ACF by 27% ($P < 0.05$) and 43% ($P < 0.01$), respectively. Moreover, the number of BCAC in Group 5 was significantly lower than that in Group 3 (76% inhibition, $P < 0.01$).

Effects of Curcumin on the Expression Levels of TNF-α, IL-6, and COX-2 mRNAs in the Colonic Mucosa of AOM-Injected *db/db* Mice

Quantitative real-time RT-PCR analysis indicated that feeding with 2% of curcumin significantly decreased the expression levels of TNF-α (Fig. 1A, $P < 0.05$) and COX-2 (Fig. 1C, $P < 0.05$) mRNAs in the colonic mucosa of AOM-injected mice relative to those of the curcumin-untreated control mice. In addition, the expression levels of IL-6 mRNA were apparently decreased to a greater extent by administration of both doses of curcumin (Fig. 1B, $P < 0.01$).

Effects of Curcumin on the Activation of AMPK and the Expression of COX-2 Proteins in the Colonic Mucosa of AOM-Injected *db/db* Mice

A Western blot analysis indicated that administration of both concentrations of curcumin caused significant phosphorylation

TABLE 1
Effects of curcumin on AOM-induced ACF and BCAC formation in the colon of male *db/db* mice

Group no.	Treatment	No. of mice	Length of colon (cm)	Total no. ACFs/colon	Total no. BCACs/cm^2
1	Saline	5	11.1 $\pm$ 0.8[a]	0	0
2	Saline + 2% curcumin	5	10.5 $\pm$ 0.2	0	0
3	AOM alone	10	10.6 $\pm$ 0.8	134.0 $\pm$ 24.5	3.4 $\pm$ 1.8
4	AOM + 0.2% curcumin	9	9.6 $\pm$ 1.6	98.2 $\pm$ 36.6[b]	1.5 $\pm$ 1.1
5	AOM + 2% curcumin	9	10.4 $\pm$ 0.4	76.4 $\pm$ 13.6[c]	0.8 $\pm$ 1.4[c]

[a]Mean $\pm$ SD.
[b]Significantly different from Group 3 ($P < 0.05$).
[c]Significantly different from Group 3 ($P < 0.01$).